Citation
Hao, H. and Tran, T.T. and Li, H. and Pham, T.M. and Chen, W. 2021. On the accuracy, reliability and controllability of impact tests of RC beams. International Journal of Impact Engineering. 157: ARTN 103979. http://doi.org/10.1016/j.ijimpeng.2021.103979

On the Accuracy, Reliability and Controllability of Impact Tests of RC Beams

Hong Hao, Tung T. Tran, Huawei Li, Thong M. Pham*, Wensu Chen*

Center for Infrastructural Monitoring and Protection, School of Civil and Mechanical Engineering, Curtin University, Kent Street, Bentley, WA 6102, Australia

*Corresponding authors: Thong M. Pham (thong.pham@curtin.edu.au) and Wensu Chen (wensu.chen@curtin.edu.au)

Abstract

The impact response of reinforced concrete (RC) beams has been intensively investigated by impact tests with various setups. Given the same impact energy, different setups of drop-weight impact tests might lead to different measurements and observations of identical RC beams including the impact force, reaction force and displacement, implying the obtained impact test results depend on not only the impact energy and structure itself, but also the test setups. Therefore, it is essential to understand the measurement accuracy, reliability, and controllability of drop-weight impact tests for a successful impact test design and interpretation of test results on RC beams. This study examines the effects of various test setups and critical factors on the impact response of RC beams. Recommendations for the processing and interpretation of test results with respect to the configuration of the test setup, including the location of load cells, mass and shape of the impact head, interlayer, and boundary condition are made for drop-weight tests. The mechanism of the negative reaction force often observed in impact tests has been unveiled for a better understanding of the impact problem.

Keywords: Impact loading; Drop-weight tests; Impact force profiles; Negative reaction forces; RC beams.

1. Introduction

Impact responses of reinforced concrete (RC) beams have been intensively investigated recently but some observed phenomena have not been well understood yet. The impact response of RC beams can be studied by using experimental testing [1-3] and/or numerical simulation [4-6]. For the experimental testing, there are a few common methods such as dropping RC beams from a certain height to the ground [7], instrumented pendulum [8], or instrumented drop-weight tests [9, 10]. Among these methods, the drop-weight tests are the most popular technique to study the impact responses of RC beams. The available drop-weight testing facilities include drop towers [11], drop-weight on site with a weight up to 2 tons [2], or instrumented drop-weight tests in laboratory conditions [2, 3, 9]. The setup of drop-weight tests has significant influences on the impact behaviour of RC beams. For example, Pham et al. [4] has reported that a minor change at the impact point (with/without using plaster) led to a tremendous variation of the peak impact force up to 300%. Li et al. [12] have observed that the drop-weight shape had a significant influence on the impact behaviour of RC beams. For identical RC beams and test setup, the maximum impact force increased with the curvature radius of the impact head but the geometry of the impact head had a negligible influence on the impulse and displacement response of the beams. Li et al. [13] carried out numerical investigations on the effects of the drop-weight mass and its configuration on the impact force. It was found that if the mass ratio of the drop-weight to the impact head was less than 20, the difference between the actual impact force and the measured impact force became considerable. The authors also suggested that the mass ratio of the drop-weight to the tested beam affected the impact force profile, leading to the impact force profile containing either only a single primary impact pulse or multiple pulses with or without a force plateau. These factors affect not only the impact test measurement results but also the beam's response, however, there has not been a systematic study that well discusses these factors in the literature. This study reviews

previous findings, carries out more simulations, and makes some comparisons to quantify the effects of these parameters on the impact responses of RC beams. Accordingly, recommendations are made to better control the impact tests and obtain more reliable measurements.

Meanwhile, the influences of support configuration, steel plate and prestress force at the support on the impact response of RC beams have not been well studied yet. For instance, the negative reaction force of a simply-supported beam subjected to impact loading was observed and reported in both the previous experimental and numerical studies [6, 9, 14]. This behaviour is very different from the RC beams under static loads, e.g., a simply-supported beam under quasi-static force does not exhibit a negative reaction force (downward direction). In previous studies [9, 10], impact tests on beams of the same design but different beam spans subjected to the same drop-weight impacts were carried out, the negative reaction force was only observed in long beams but not in short beams. The appearance of negative reaction forces was attributed to stress wave propagations [9, 15] but there was neither experimental nor numerical evidence to support the explanation. Therefore, it is necessary to unveil this phenomenon and investigate how it affects the impact response of RC beams. This study develops high-fidelity finite element (FE) models to study the phenomenon and the cause of the negative reaction force. In addition, the effect of another factor, i.e. the support configuration on the impact response is also examined. Recommendations for processing and interpretation of measured data are also presented.

2. Impact force

The impact force measured by various methods is primarily determined by the contact stiffness and impact energy [16, 17]. Given the identical impact energy, drop-weight test setup configurations that result in various contact stiffness (through different contact areas and

material properties) would cause very different impact forces. Since the impact force governs the failure mode and dynamic response of RC beams, it is essential to properly measure the impact force acting on RC beams and thus predict their dynamic responses. Therefore, accurate measurements of the impact force is essential. The commonly adopted impact force measurement methods are summarized first in this section, and then the effects of different test setup configurations on the impact force measurements are presented. The impact force profiles and failure mode of RC beams are also categorized and discussed. It should be noted that most of the results and findings in this section are reviewed based on the previous studies [4, 12, 13, 16, 18, 19] and systematically summarized herein for a better understanding of the impact problem.

2.1. Impact force measurement

The impact force could be measured by indirect or direct methods [13]. Fig. 1(a) and (b) show the indirect methods, which derive the impact force by using inverse analysis. For the first indirect method as presented in Fig. 1(a), the impact force is calculated as the multiplication of drop-weight mass and its acceleration. The acceleration of drop-weight during impact usually shows significant fluctuation and it can be captured by accelerometers directly attached to the drop-weight [14, 20]. For the second indirect measurement method based on d'Alembert principle [1, 21], the impact force is obtained by the sum of inertia force along the beam and the reaction force at beam ends as shown in Fig. 1(b). The inertia force along the beam is determined by the acceleration and mass along the beam. However, the stress wave propagated in the drop-weight and along the beam might affect the measurement accuracy of the captured acceleration and thus influence the accuracy of the acquired impact force. Therefore, load cells (strain gauge type [9, 10, 22-25] or piezoelectric type [26, 27]) as a direct method have been more often employed to record the impact force in many impact tests. The load cell can be embedded into the drop-weight (Fig. 1(c)) or placed on the tested beam (Fig. 1(d)).

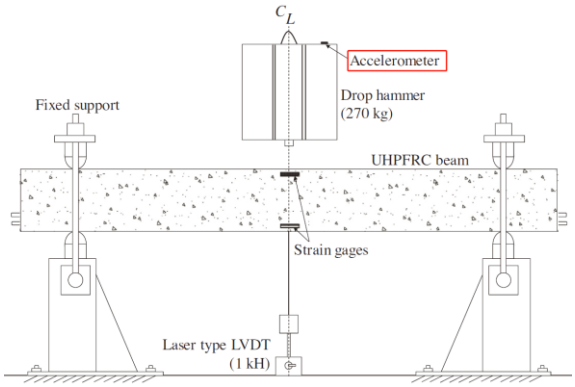

(a) Impact force indirectly obtained by acceleration of drop-weight [20]

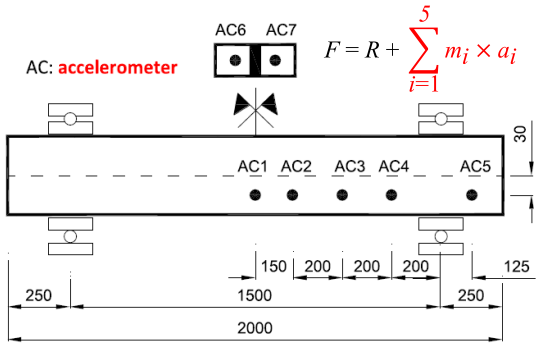

(b) Impact force indirectly obtained by acceleration along the beam and reaction force [21]

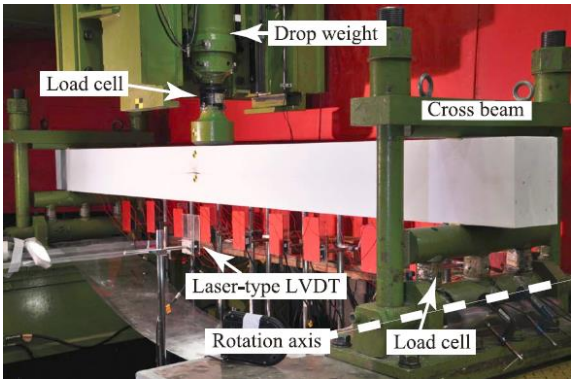

(c) Impact force directly recorded by load cell embedded in drop-weight [28]

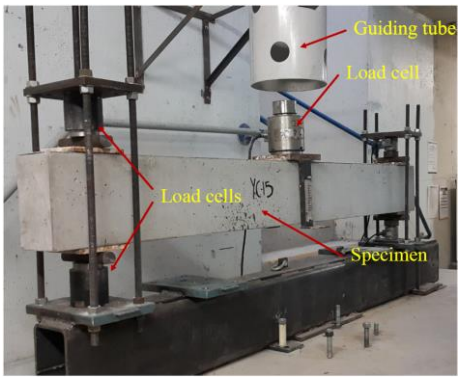

(d) Impact force directly recorded by load cell placed on beam [15]

Fig. 1. Different methods of impact force measurement

2.2. Measurement accuracy

When a load cell embedded into the drop-weight is used to measure impact force as shown in Fig. 2, the measured impact force is always lower than the actual contact force (F_c) owing to the inertia effect of the drop-weight head (F_{ih}) [13]. Therefore, the accuracy of the measured impact force is affected by the drop-weight mass distribution. To quantify the effect of drop-weight mass distribution on the measurement accuracy of impact force, the drop-weight mass ratio ($\alpha_d = \frac{m_w}{m_h}$), in which m_w and m_h are respectively the mass of the weight and the impact head, was considered in the previous study [13]. The numerical models in Ref. [13] were developed in LS-DYNA and calibrated by the drop-weight impact tests conducted by Fujikake et al. [3]. The impacted beams had the identical beam span of 1.4 m, beam cross-section (250 mm in depth and 150 mm in width) and rebar layout as given in Ref. [3]. The entire drop-weight was

kept as 400 kg, while the mass of weight and the mass of impact head were set to meet the designed drop-weight mass ratios (e.g. 0.5, 1.0, 20.0, and 50.0) by adjusting material density. The drop-weight impacted the simply-supported beam directly at midspan at a velocity of 4.85 m/s for all cases. In the numerical models, the concrete beam, drop-weight, and load cell were simulated by the constant stress solid elements with a single integration point. The Hughes-Liu beam element with 2 × 2 Gauss quadrature integration was employed to simulate the longitudinal rebars and stirrups. The KCC concrete model (i.e., Mat_72R3 in LS-DYNA) that considered the strain rate of concrete was adopted for the concrete beam. The steel rebars were modelled by the elastic-plastic steel model (i.e., MAT_24). Moreover, the longitudinal rebars and stirrups were embedded into the concrete beam by using the beam-in-solid constraint method. The mesh size of 10 mm for the numerical models was adopted after conducting a mesh convergence study to obtain reliable results with reasonable computational efficiency. The same numerical simulation techniques are employed in the following sections. More detailed information of numerical models is not given herein but can refer to Ref. [13]. The reported impact force (F_{lc}) extracted from the axial force of the load cell at the mid-height (as shown in Fig. 2) was compared with the actual contact force (F_c) obtained directly from the numerical model.

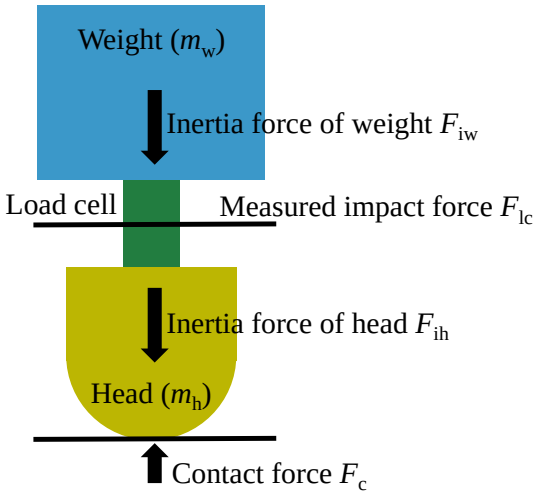

Fig. 2. Force equilibrium analysis of drop-weight

For better illustration of the influence of drop-weight mass distribution on the measurement accuracy, the actual contact force (F_c) and the measured impact force (F_{lc}) under the drop-weight mass ratios of 0.5, 1.0, 20.0, and 50.0 obtained in Ref. [13] were extracted, re-compiled and shown in Fig. 3. The measured impact force agreed well with the actual contact force when α_d was higher than 20, but the measured impact force was significantly lower than the actual contact force when α_d was lower than 1. In other words, the measured impact force deviated from the actual contact force acting on the beam, indicating inaccurate impact force measurements. Therefore, a reasonable drop-weight mass ratio (α_d) should be employed when the impact force is measured by a load cell embedded in the drop-weight. If a lighter drop-weight was employed in the test, it would lead to a lower drop-weight mass ratio (α_d) and thus a larger discrepancy between the actual contact force and the measured impact force. Thus, the measured impact force should be corrected to obtain a more accurate impact force. A correction method based on analytical derivations to correct the measured impact force can be found in the previous study by Li et al. [13].

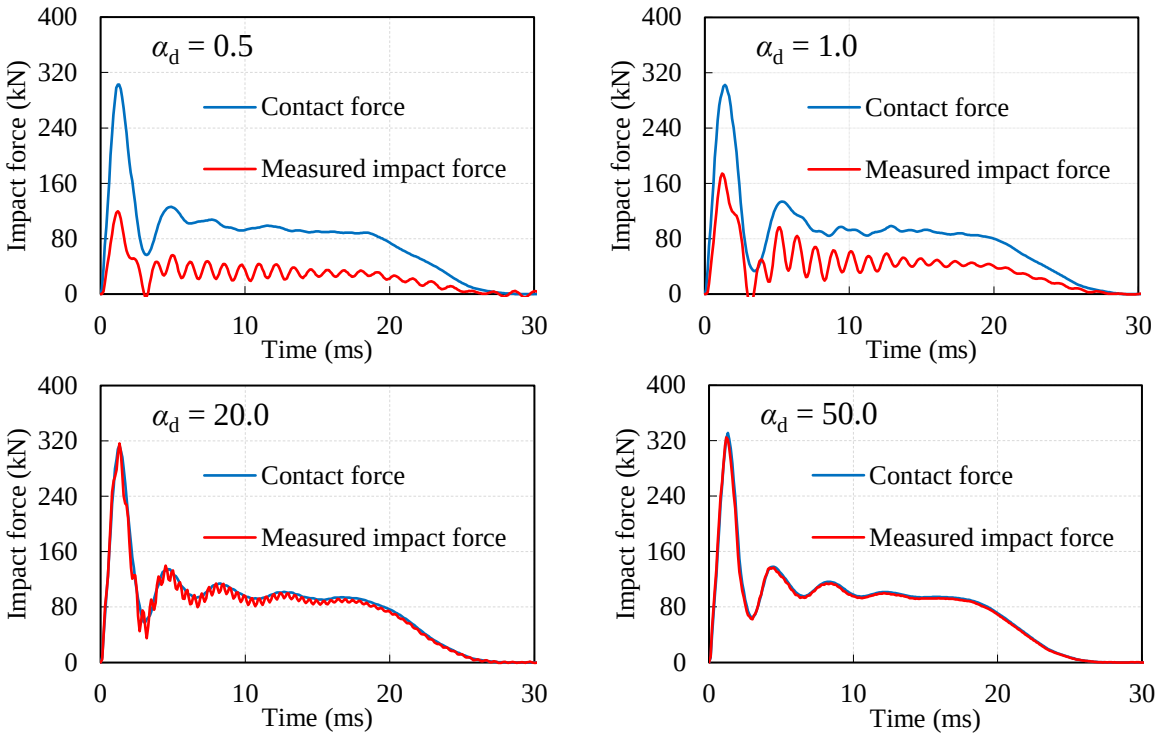

Fig. 3. Contact force and measured impact force

2.3. Influence of load cell position

The load cell to measure the impact force could be installed in the drop-weight or placed on the beam as presented in Fig. 1. It has been found that the drop-weight mass ratio would affect the accuracy of the measured impact force if the load cell is mounted inside the drop-weight. Moreover, the contact stiffness and the impact force value change if the load cell is placed on the beam [12, 16]. Li et al. [13] numerically quantified the influence of load cell position on the impact force by comparing the measured impact force through load cells at different locations, i.e., embedded in the drop-weight and placed on the beam as show in Fig. 4. In the numerical models, the RC beams had the identical dimension and rebar layout as employed in Section 2.2. The beam had a span of 1.4 m, depth of 250 mm, and width of 150 mm. The impact mass was 400 kg and the impact velocity was 4.85 m/s. The drop-weight mass ratio (α_d) of 50 was employed for the specimen in Fig. 4(a) to reduce the effect of drop-weight mass distribution on the measurement accuracy [13].

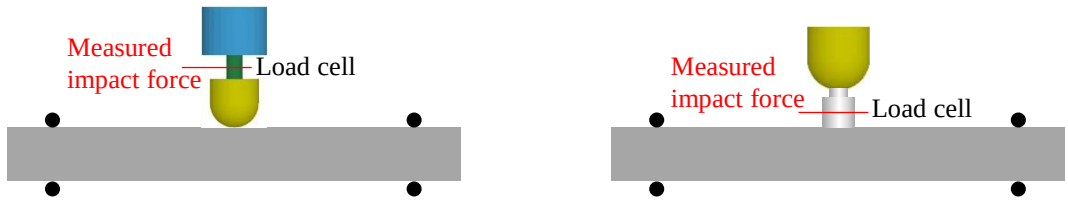

(a) Load cell I: load cell installed in drop-weight (b) Load cell II: load cell placed on beam

Fig. 4. Different load cell positions

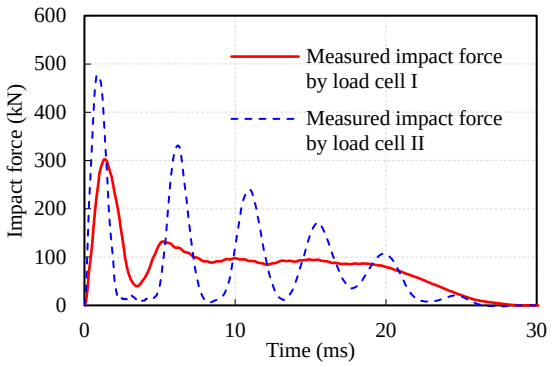

Fig. 5. Impact force measured by load cell at different positions

For better demonstration of the effect of load cell positions, the impact forces measured by the load cells located at different positions in the previous study [13] were replotted and shown in Fig. 5. The impact force profile with a primary impulse and a force plateau was recorded by the Load cell I while multiple secondary peaks following a primary impulse were measured by the Load cell II. Moreover, a higher loading rate at the initial stage of an impact event was observed when the load cell was placed on the beam. The measured peak impact force of 477 kN by the load cell II was 58% higher than that of 302 kN by the load cell I, due to the increased contact stiffness generated by the load cell placed on the RC beam, as well as the inertial resistance of the impact head which reduces the measured impact force as discussed above. These results indicate that besides the different contributions of the inertial force from the impact head, placing the load cell on beam changes the contact stiffness, which leads to the changes of the impact force acting on the beam.

2.4. Influence of impact head geometry

Fig. 6 shows the impact heads with various geometries [12, 29], such as hemispherical head [17, 30], curved heads with a certain radius [2, 28], and flat head [31-34] commonly used in drop-weight impact tests. Upon impact, different impact heads have different contact areas between the beam and the drop-weight [12, 18]. The change of the contact area could induce different contact stiffness and change the impact force. It is difficult to compare the effect of impact head geometry directly by using the available testing results since the impact energy, dimension of beams, and material strength were not consistent in these tests. To investigate the influence of the impact head geometry on the impact force, Li et al. [12] developed numerical models of RC beam that were impacted directly by drop-weight head with different geometries. The numerical models of simply-supported RC beam had the same geometry dimension (span of 2.9 m, width of 200 mm and height of 400 mm) and rebar layout as those in the test [35]. The impact mass was 253 kg and the impact velocity was 6.86 m/s.

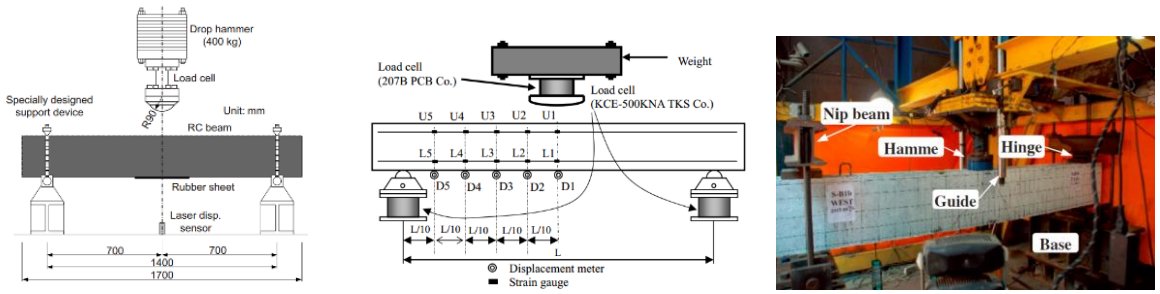

(a) Hemispherical head [3] (b) Curved head [36] (c) Flat head [34]

Fig. 6. Different impact head geometries in previous tests.

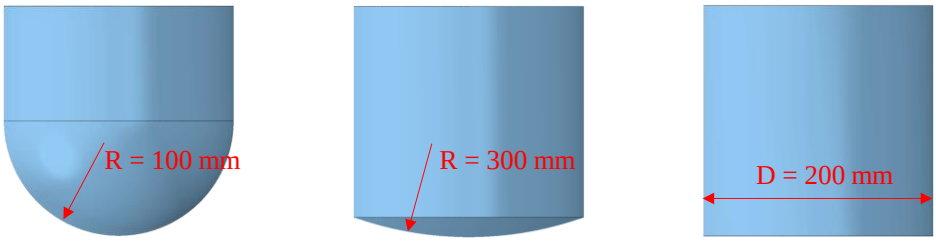

Hemispherical head Curved head Flat head

Fig. 7. Impact head geometries

To better illustrate the effect of drop-weight head geometry, the impact forces generated by three drop-weight heads (i.e., hemispherical head, curved head, and flat head as shown in Fig. 7) were extracted from Ref. [12] and shown in Fig. 8. The results showed that primary impact force peaks for the hemispherical head, curved head, and flat head were 987 kN, 1365 kN, and 2561 kN, respectively, with a variation of 160% between the maximum primary peak (flat head) and the minimum primary peak (hemispherical head) [12]. In addition, the duration of the primary impulse increased as the drop-weight head changed from flat head to hemispherical head. The flat head induced the highest loading rate and thus caused the highest peak impact force and the shortest impact duration. Accordingly, the impact force could be controlled by using different drop-weight head geometries. Therefore, if a higher peak impact force with a shorter duration is expected to be applied on a beam, the drop-weight head with a larger contact area (e.g. flat head) should be employed, and vice versa. However, it should be noted that the hemispherical and curved heads subjected to relatively higher impact velocity could induce

more severe local concrete damage at the impact zone with more severe indentation damage to concrete [12].

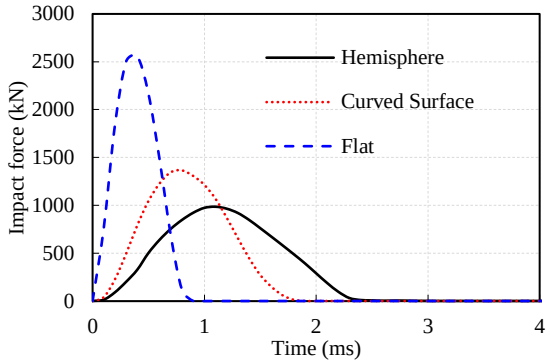

Fig. 8. Impact force generated by different impact head geometries with the same drop-weight mass and velocity

2.5. Influence of initial inclination of drop-weight

In the previous drop-weight impact tests, the drop-weight vertically falls freely or along guide rails to impact the beam specimen at midspan [1, 12, 18]. Ideally, the center line of the drop-weight coincides with that of the beam as shown in Fig. 9(a) when the drop-weight begins to contact the beam. However, an angle between the center lines of drop-weight and beam θ, i.e., initial inclination as shown in Fig. 9(b), may exist in the tests [12, 37]. Li et al. [18] found that a slight initial inclination of the drop-weight with a flat head would reduce the contact area of the drop-weight with the beam, and led to changes in the impact scenario and beam responses. To verify the influence of initial inclination of drop-weight on the contact area and impact force, the drop-weight with a flat head or a hemispherical head was employed to directly impact the RC beam at midspan by the authors [12]. In the numerical studies, the initial inclination angles of 0°, 1°, and 2° were considered. It is worth noting that the inclination angle of 0° stands for the ideal impact as shown in Fig. 9(a). The RC beams in the numerical models had the same dimension, material strength, and rebar layout as those presented in Section 2.4 (span of 2.9 m, width of 200 mm and height of 400 mm). The drop-weight with a mass of 253 kg directly impacted the beam with a downward velocity of 6.86 m/s.

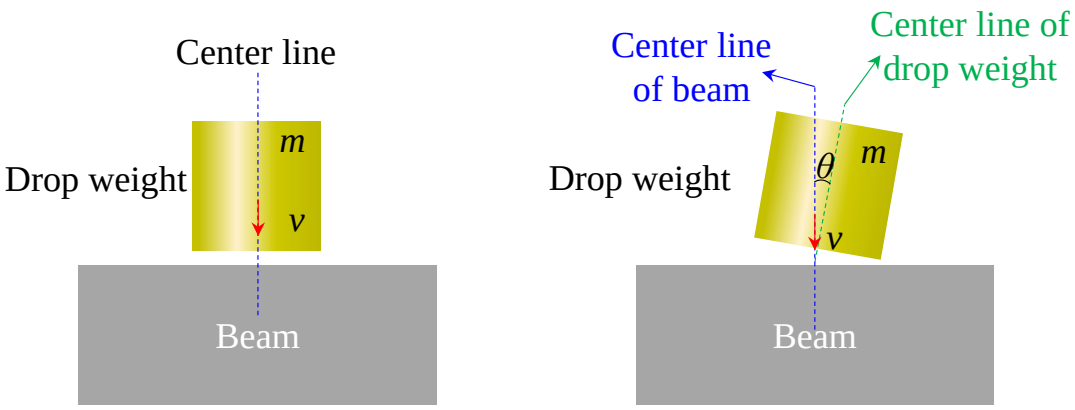

(a) Ideal impact (b) Impact with initial inclination

Fig. 9. Ideal impact and impact with initial inclination

The time histories of impact force generated by drop-weight with different initial inclinations as reported in [12] were replotted and presented in Fig. 10. The peak impact forces of specimens impacted by the hemispherical head were 987 kN, 993 kN, and 977 kN for the initial inclination angles of 0°, 1°, and 2°, respectively, with a very minor variation of 1.6% as presented in Fig. 10(a). This is because the initial inclination of drop-weight with hemispherical head or curved head had very limited effect on the contact area and thus induced a negligible influence on the impact force [12]. In contrast, if the beam was impacted by the flat head, the peak impact forces were 2561 kN, 1878 kN, and 1251 kN, respectively, as illustrated in Fig. 10(b), which presents a difference of 51%. The duration of the primary impulse increased by 122%, from 0.9 ms under the ideal impact (0°) to 2.0 ms under the impact with an initial inclination of 2°. In other words, the flat head with a small initial inclination angle could cause a significant variation in the impact duration and peak impact force. It was because the flat head with a larger inclination angle would reduce the contact area of the impactor with the beam. Accordingly, the smaller contact area led to a lower contact stiffness and a decrease in the impact force. Therefore, the possible initial inclination angle should be taken into consideration in the drop-weight test setup if a flat head is used. Using a curved surface could reduce the influence of the initial inclination on the impact force.

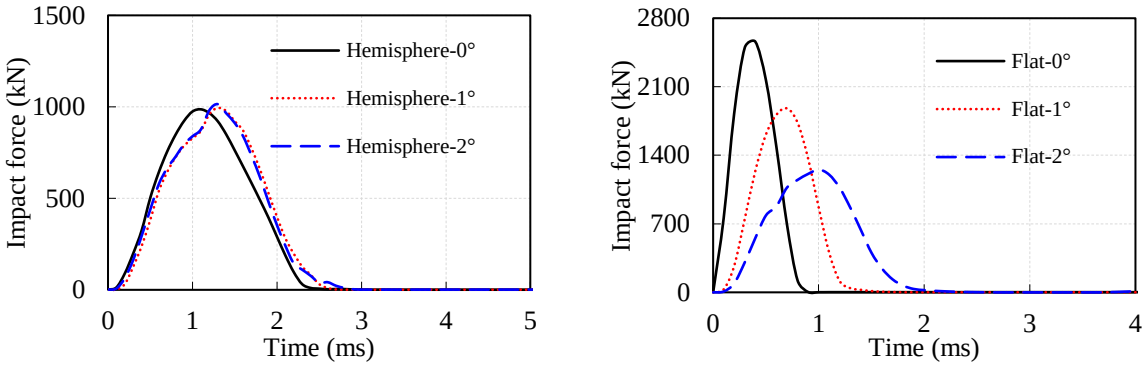

(a) By hemispherical head (b) By flat head

Fig. 10. Impact force by considering initial inclination angle

2.6. Influence of impact interlayer

Besides the direct impact induced by drop-weight [2, 3, 30, 35, 36, 38], various interlayers placed between the beam and the drop-weight have been used in drop-weight impact tests but its effect on the response of the beams has not been well understood. The common impact interlayers include steel plates [1, 17], rubber pads [39], or plywood pads [40]. The steel plates or plywood pads were used to prevent premature local damage at the impact zone and achieve even contact [1, 11, 17], while the rubber pads were employed to reduce the oscillations and local damage [11, 31, 39]. However, it should be noted that the interlayers with different properties yield various contact stiffness thus change the impact force [4, 17, 41]. Li et al. [12] numerically quantified the influence of the impact interlayer on the impact force by placing various interlayers with different thickness as presented in Fig. 11. The beam had a span of 2.9 m, width of 200 mm and height of 400 mm. The drop-weight with a mass of 253 kg and a velocity of 6.86 m/s impacted the beam directly or indirectly impacted via the interlayers.

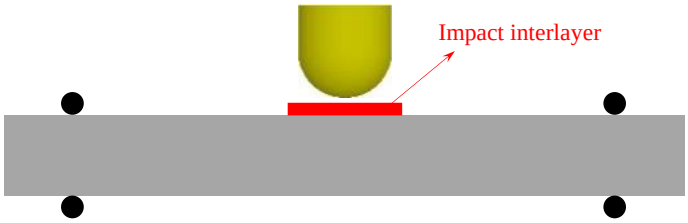

Fig. 11. Beam with impact interlayer

The impact forces induced by the direct impact and the indirect impact via steel plate, hard rubber pad, and soft rubber pad with a thickness of 40 mm reported in [12] were extracted, re-compiled, and shown in Fig. 12. It can be seen that using the steel plate led to 285%, 246%, and 82% higher impact force peak than using the soft rubber pad, the harder rubber pad, and the direct impact, respectively [12]. The harder contact condition induced a higher loading rate, a higher peak impact force, and shorter duration. The higher loading rate led to a more significant inertia effect of the tested beam and caused more severe damage at the negative bending moment area [12]. In contrast, softer contact decreased the loading rate and impact force, and prolonged the impulse duration. The lower loading rate reduced the inertial effect of the beam and therefore made the beam more likely to experience a flexural-governed failure mode. To sum up, using different impact interlayers at the impact zone causes different impact loading rates and impact impulses acting on the beam. An interlayer with the proper hardness and thickness of interlayer should be adopted to achieve the desired contact scenario in the drop-weight impact tests.

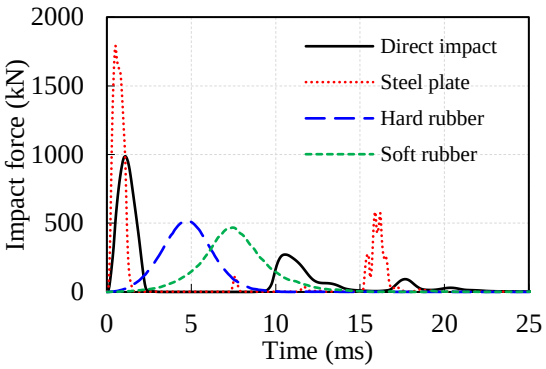

Fig. 12. Impact force by using different interlayers

2.7. Impact force profile and structural response

A previous study by the authors [13] examined the testing results available in the literature [14, 17, 31, 34, 35, 42] and performed intensive numerical simulations. Based on both the experimental and numerical results, it was concluded that the impact force profiles can be classified into three types (Type I, II, and III) as presented in Fig. 13. The primary force peak

of three impact force profiles is caused by the contact between beam and drop-weight at the early stage of impact [4, 5]. The secondary peaks and force plateau of the impact force profiles (Type II and III) are governed by the relative motion of beam and drop-weight following the primary impulse. The impact force profiles are affected by the impact mass ratio ($\alpha = \frac{m_d}{m_b}$) of the entire drop-weight mass (m_d) to beam mass (m_b), which was numerically studied in Ref. [13]. In the numerical simulations, the simply-supported RC beam with the identical mass of 131.25 kg was impacted by drop-weight with various mass to produce the impact mass ratios (α) from 0.25 to 4.0. The beam had a span of 1.4 m, depth of 250 mm, and width of 150 mm. The impact velocity was kept as 4.85 m/s. More detailed informaiton and results can refer to Ref. [13].

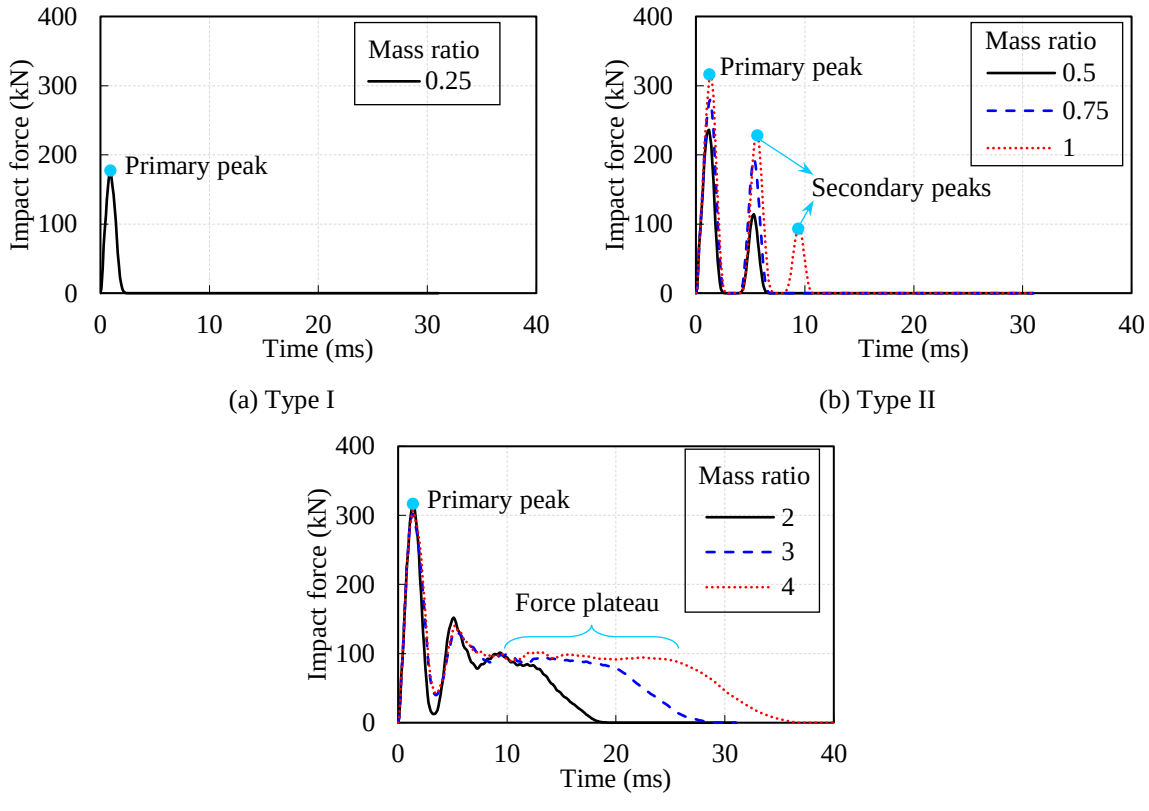

(a) Type I

(b) Type II

(c) Type III

Fig. 13. Typical impact force profiles by considering various mass ratios

For better illustration of the influence of impact mass ratio on the impact force profiles, the impact force generated by considering the impact mass ratios in the range of 0.25 to 4.0 obtained

in Ref. [13] were extracted, re-compiled and shown in Fig. 13. As depicted in Fig. 13(a), the impact mass ratio of 0.25 led to the Type I impact force profile. The impact force profile (Type II) with a primary force peak followed by one secondary peak (α = 0.5 and 0.75) or two secondary peaks (α = 1.0) was observed in Fig. 13(b). For the impact mass ratios of 2.0 to 4.0, the impact force profile (Type III) exhibited a force plateau following the primary impulse as depicted in Fig. 13(c). Therefore, the impact force profile can be tailored by adjusting the ratio of impact mass to specimen mass. The impact force profile would have a force plateau when a heavy drop-weight (i.e., with a higher impact mass ratio) impacts a light beam. Additionally, when the beam moves downwards after the primary impulse and generates vertical displacement at the midspan, the global stiffness of the beam is mobilized with the deformation of the beam. The beam with higher global stiffness (e.g. smaller beam span or beam ends with more constraints) leads to a higher secondary peak or force plateau [16].

To understand structural response under different impact force profiles, the time histories of impact force and displacement at midspan are presented in Fig. 14. The maximum displacement increases with the impact mass ratio. For the displacement induced by Type II impact force profile, the maximum displacement appears either before or after the secondary peaks, depending on the global stiffness of the beam and impact energy. For higher global stiffness of the beam and impact energy, the maximum displacement usually appears after the secondary peaks [18], which can cause a local zigzag of displacement profile before reaching the maximum displacement as depicted in Fig. 14(b) due to the secondary impact. This phenomenon was also observed in the numerical and experimental results [43-45]. Meanwhile, the maximum displacement induced by Type III impact force profile always occurs at the end of the force plateau as presented in Fig. 14(c). In general, Type I impact force profile is less likely to be observed in tests, while the other two types are often observed because a heavier drop-weight is usually employed to examine the impact load-carrying capacity of beams. The

damage modes such as flexural-governed failure, flexure-shear combined, shear-governed can be predicated by a given impact force and beam design, which is discussed in the following section.

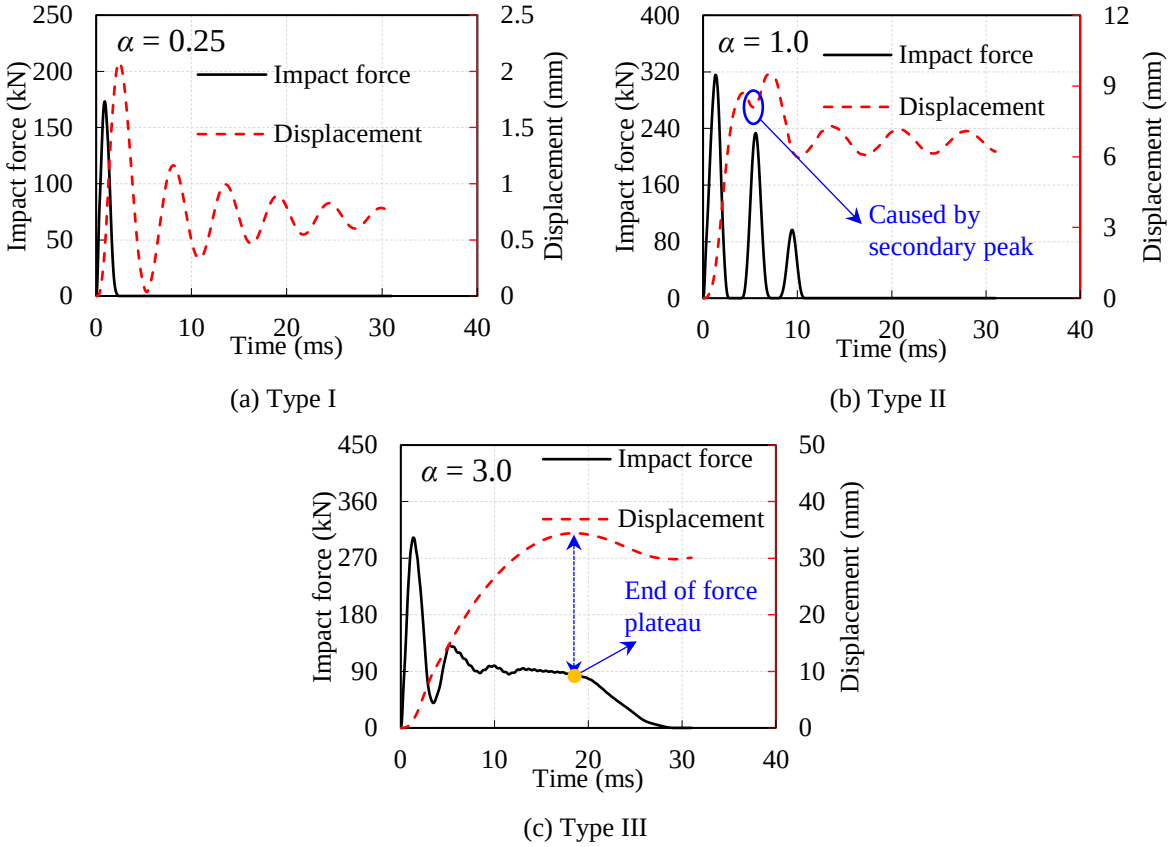

Fig. 14. Time histories of impact force and displacement at midspan

2.8. Impact force and damage mode

Damage modes of RC beams depend on their impact load-carrying capacity and the impact force applied on the beam [19, 46-48]. Fu et al. [49] found that RC beams experienced flexural-governed, combined flexure-shear, shear-governed, or punching shear failure, with the increased impact velocity. Moreover, under an impulse with a higher impact force peak and shorter duration, RC beams are prone to suffer the shear-governed or punching shear damage. In addition, a lighter drop-weight with a higher impact velocity, generating Type II impact force profile, is more likely to induce a shear-governed or punching shear failure [12, 17, 18, 35, 49], while a flexural failure or flexural-shear combined failure usually associates with Type III impact force profile [3, 17, 49]. Fig. 15 shows a typical punching shear failure, which

demonstrates the failure section with diagonal cracks of 45° [1, 47, 49]. The beam would experience punching shear failure [19] if the dynamic shear load-capacity of beam section $P_{\mathrm{dyn}}^{\max}$ is less than the peak impact force. An analytical method to calculate $P_{\mathrm{dyn}}^{\max}$ with consideration of strain rate effect and inertia effect of the shear plug can be referred to Ref. [19]. Therefore, the punching shear failure of RC beams under impact loading can be predicted by comparing the peak impact force and the calculated $P_{\mathrm{dyn}}^{\max}$.

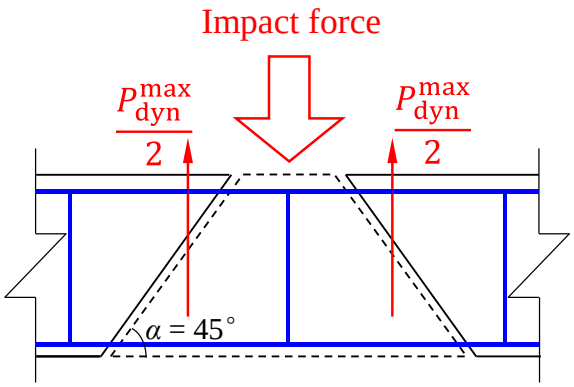

Fig. 15. Schematic diagram of punching shear failure

The damage modes at the negative bending moment regions of two identical simply-supported beams subjected to different impact forces are different as presented in Fig. 16. By analysing the impact force profile acting on the beams, it can be found that the impact force with a higher primary force peak and shorter duration induces more flexural concrete cracks or more severe damage at the negative bending moment areas. It is because the impact force with a higher primary force peak and shorter duration mobilizes a larger inertia resistance of the beam during the primary impulse [4]. It is noted that in the early state only a portion of the beam is activated while the remaining parts are still stationary. These two parts are divided by a stationary point which was clearly defined and discussed in the previous study [45]. The two stationary points act as “fixed restraint” and thus induce the negative bending moment under impact loading. Accordingly, the higher peak impact force, the higher negative bending moment. Proper design by adjusting the impact force is needed to avoid the unexpected excessive damage at the negative bending moment area.

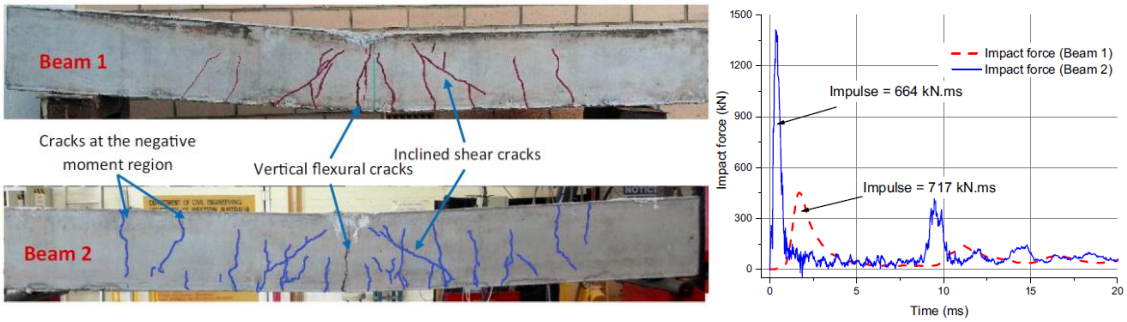

(a) Test result in Ref. [4]

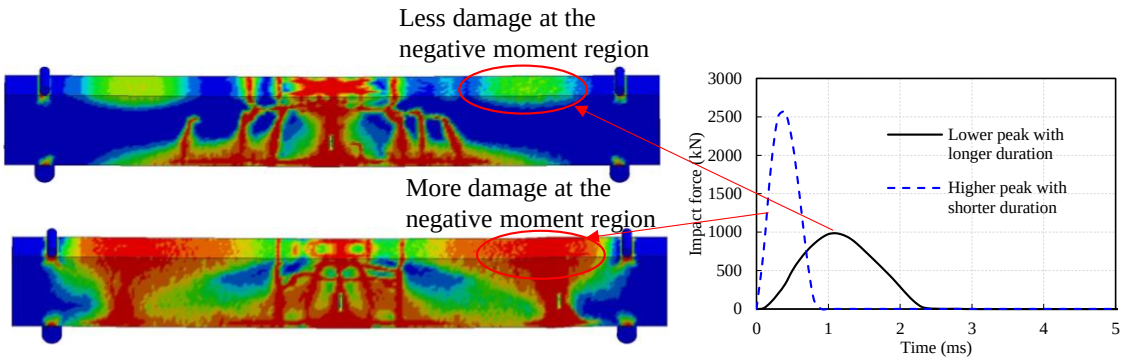

(b) Numerical result in Ref. [12]

Fig. 16. Impact force and damage at the negative moment region

3. Reaction force

3.1. Cause of negative reaction force

The reaction force of RC beams subjected to impact loading is normally measured by load cells. The setup for impact tests is different from the static case where a simply-supported beam under quasi-static loads requires restraint against downward movement only. On the other hand, the setup of a simply-supported beam subjected to impact loading requires restraints from both downward and upward movement at supports because the impacted beam not only deforms downward but also rebounds upward. Accordingly, under impact tests, both negative and positive reaction forces need to be monitored during the impact test. Interestingly, not many previous studies measured the negative reaction force [6, 9, 10, 38]. Among those studies that measured the reaction forces, some studies reported the negative reaction force [9] while other studies did not observe the negative reaction force [10]. For example, Pham et al. [4, 9, 10]

tested RC beams with the same cross-section (150 × 250 mm) but different effective spans (1.9 m and 1.1 m). The 1.9 m RC beams exhibited the negative reaction force while only the positive reaction force was observed when testing the 1.1 m RC beams as shown in Fig. 17. The exact reason for this phenomenon has not been documented although there are a few attempts to explain this, based on the stress wave propagation [9] and up-lifting of the beams [38]. To better understand and explain this unique phenomenon, this section presents a numerical investigation to unveil the mechanism behind this phenomenon, and examine whether it is caused by the stress wave propagation or the global structural response. Upon improving the understanding of this phenomenon, a suggestion for the setup of simply-supported beams for impact loading test is made.

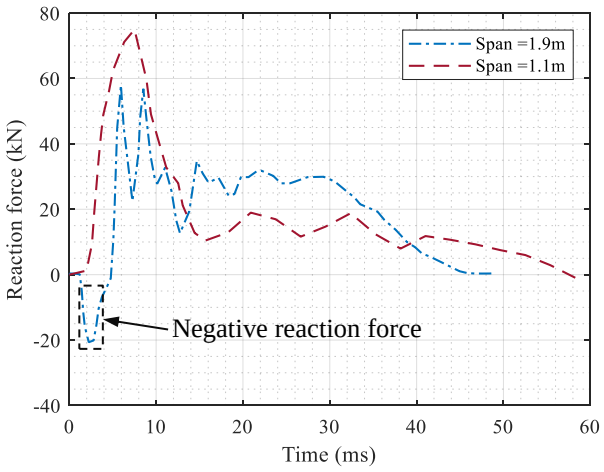

Fig. 17. Reaction forces of RC beams with different spans (1.1 m and 1.9 m)

The numerical model of the RC beam developed in the previous study [4] was used for the investigation and as a reference model for extensive numerical simulations presented in subsequent sections (see Fig. 18(a)). The beam had rectangular section of 150 mm in width and 250 mm in height. The span length of this simply-supported beam was 1.9 m. All nodes of the steel plates on the top of upper rollers, the steel plates under lower rollers, and rollers were fixed in all degrees of freedom on both sides of the beams (as shown in Fig 18a). The steel plates

adjacent to the beam surface can rotate freely around the rollers. The mass of projectile and impact velocity were 200 kg and 6.26 m/s respectively. The CONTACT_AUTOMATIC_SURFACE_TO_SURFACE option along with the standard penalty formulation (SOFT = 0) was adopted to all contacts in the model. In this contact model, the friction coefficient is time-dependant and invoked by the static friction coefficient, μ_s and then decay exponentially to dynamic friction coefficient, μ_d as presented below [50]:

$$\mu = \mu_d + (\mu_s - \mu_d)e^{-c|v|} \quad (1)$$

where c is the decay constant and v is the relative velocity between slave node and master segments. In LS-DYNA, the input parameters for modelling friction between the steel rollers with steel plates, and the steel plates with concrete surfaces are presented in Table 1. Meanwhile, the parameters for the remaining contact models and material models can be found in the previous study [4]. The model was developed in LS-DYNA and its accuracy was verified against the experimental results with a good agreement [4]. The time histories of impact force, the top (negative) and bottom (positive) reaction forces, and resultant reaction force (sum of the top and bottom reaction forces) obtained from numerical results are presented in Fig. 18. It can be seen from the figure, the top reaction force was activated before the bottom reaction force. This result has confirmed the observations of the negative reaction force in the previous experiments [6, 9, 38].

Table 1. Parameters for simulating the contacts at supports

Contact	SFS/SFM	Static friction coefficient	Dynamic friction coefficient
Steel rollers (SFS)/Steel plates (SFM)	1/1	0.8	0.6
Steel plates (SFS)/Concrete (SFM)	0.1/0.001	0.6	0.3

*SFS: scale factor of slave elements and *SFM: scale factor of master elements

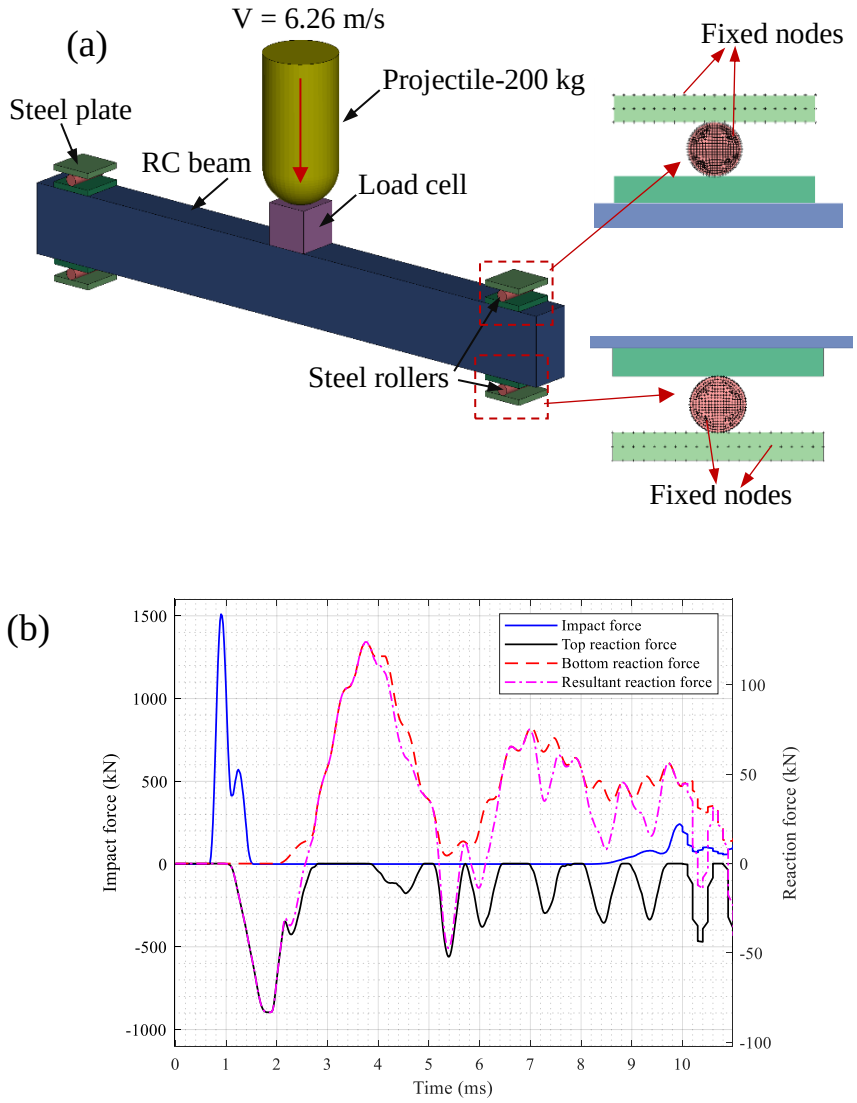

Fig. 18. (a) FEM model of the RC beam and (b) numerical result of the histories of forces

A series of simulations with a change of the impact velocity, mass of the drop-weight, and span length were carried out to investigate their effects on the negative reaction force. The effect of impact velocity, projectile mass, and span length on the resultant reaction force is visualized in Fig. 19. It can be seen that the positive reaction force was not significantly affected by the variation in impact velocity, projectile mass, and span length of the beams. Meanwhile, the negative reaction force increased with the impact velocity and projectile mass. Interestingly, the decrease in span length of the beams resulted in a reduction in the negative reaction force,

which was similar to the phenomenon reported in the previous experimental studies [9, 10]. As mentioned previously, the negative reaction force may be caused by the global deformation response or surface Rayleigh wave propagation [51]. To evaluate the significance of the surface wave propagation on the beam responses, the deformations on the same beam section at the top, center and bottom points are checked. If the surface wave propagation effect is prominent to cause the negative reaction force at the supports, the deformation at those three points should be different. On the other hand, if the deformations at those three points of the same beam section are the same, indicating the global response of the beam dominates the deformation response, the negative reaction force is therefore unlikely caused by the wave propagation in the beam.

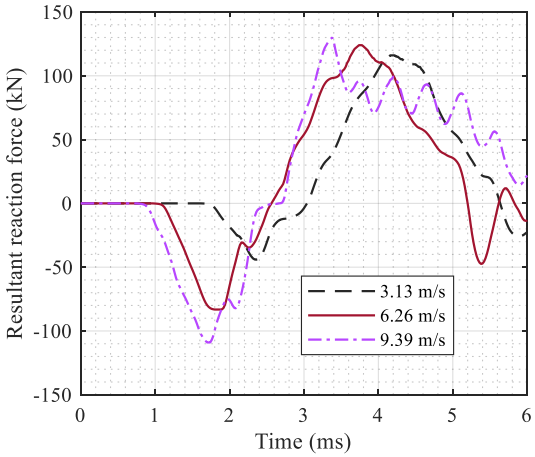

(a) Effect of impact velocity (span length =1.9 m, drop-weight mass = 200 kg)

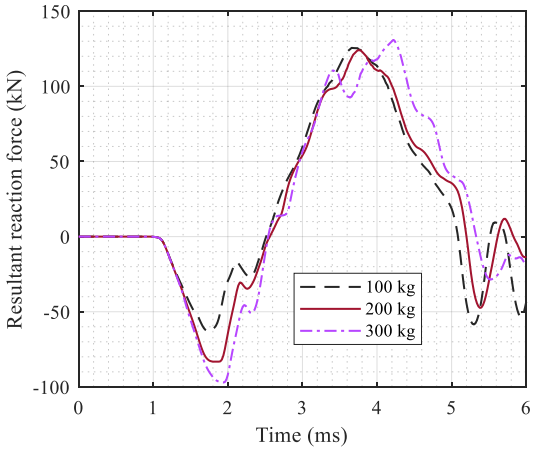

(b) Effect of projectile mass (span length = 1.9 m, impact velocity = 6.26 m/s)

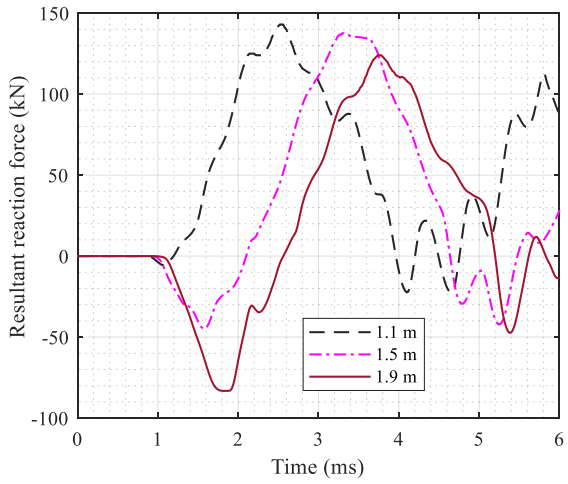

(c) Effect of the beam span (impact velocity = 6.26 m/s, drop-weight mass = 200kg)

Fig. 19. Factors influencing the reaction force

To clarify this mechanism, the deformation along the longitudinal direction of the beams at three different locations of the horizontal axis (see Fig. 20) is considered. It is noted that the beam had a cross-section of 150 × 250 mm, the span length of 1.9 m, the impact velocity of 6.26 m/s, and the drop-weight mass of 200 kg. The deformation of the beam at the center, top, and bottom axes at the impact point was very different during the early stages as shown in Fig. 21(a-b). This behaviour is primarily attributed to the indentation at the beam's top surface that led to significant higher deformation at the beam top as compared to the center and bottom surface. Apart from that area, the vertical displacements of the beams along the center, top, and bottom axes were similar. Such a phenomenon implied that during the early stage, the local response of the beams was primarily caused by the beam deflection and local indentation at the impact point rather than stress wave propagation. At the moment t_3 = 1.05 ms when the negative reaction force has just activated, the beam deformed with a high-order deformation mode, and the responded-portion of the beam has just reached the support as shown in Fig. 21(c). After that, the beam portion at the support tended to move upward (Fig. 21(d)), and the negative reaction force increased until reaching the peak when the deformation of the beam shifted to

the first mode at t_5 = 1.8 ms (Fig. 21(e)). It is noted that the time instant t_3 and t_5 respectively correspond to the activation and peak of the negative reaction force as shown in Fig. 21(f). Based on those observations, it can be inferred that the negative reaction force can be attributed to the deformation of the beam associated with high-order mode shapes. The activation of the mode shapes is governed by the natural frequencies of beams and the impact energy. Accordingly, the impact force of the beams with a span length of 1.9 m and 1.1 m is presented in the frequency domain as shown in Fig. 22. The notations f_1,f_3, and f_5 in the figure represent the natural frequencies of the first, third, and fifth mode shapes of the simply-supported beam, respectively. The estimation of those natural frequencies is based on Eq. (2) expressed as follows [52]:

$$f_n = \frac{K_n}{2\pi}\sqrt{\frac{EI}{ml^4}} \tag{2}$$

where E is the modulus of elasticity; I is the area moment of inertia; m is the mass per unit length; l is the span length; and K_n is a constant equal to $(n\pi)^2$ where n refers to the mode of vibration. Since the beams were subjected to impact load at midspan, only symmetric modes contributed to the beam vibration, therefore antisymmetric mode 2 and 4 were not considered. It can be seen from Fig. 22(a), in 1.9-m beam, the natural frequencies of the first and third modes were within the range of dominant frequencies of the impact force (0-4 kHz) with the significant magnitudes. Therefore, the vibration mode of that beam was mainly the superposition of the first and third modes as illustrated in Fig. 23 in which the deformation composition due to the third mode can lead to the negative reaction force. Meanwhile, in the case of the beam with the span length of 1.1 m, only the first mode had the significant magnitude while the magnitude of the third mode was very small which implies that the third mode had an insignificant contribution to the vibration of the beam. This explains why the negative reaction

force was negligible in this beam. Therefore, upon impact, if the third or higher vibration mode is activated and contributed significantly to the response of the beam, the negative reaction force is expected. A comparison of the beam deformation with different span lengths at the moment when negative reaction activated is presented in Fig. 24 to confirm this mechanism. In general, the negative reaction force is caused by the deformation of the beams associated with high-order mode shapes.

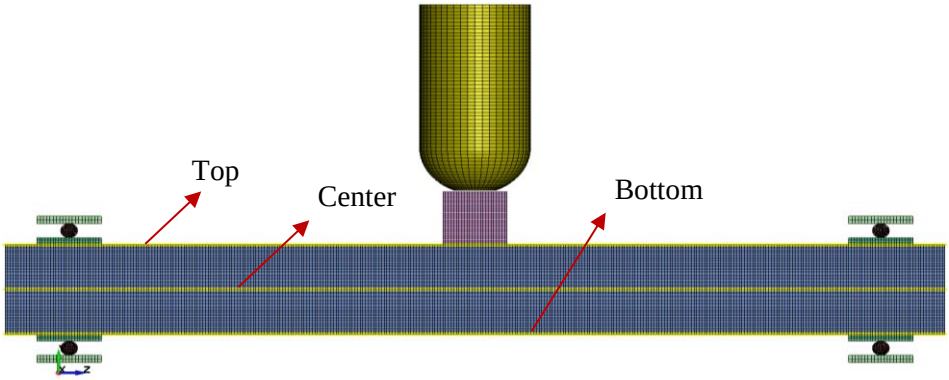

Fig. 20. Location of horizontal axes for plotting the deformation of the beam

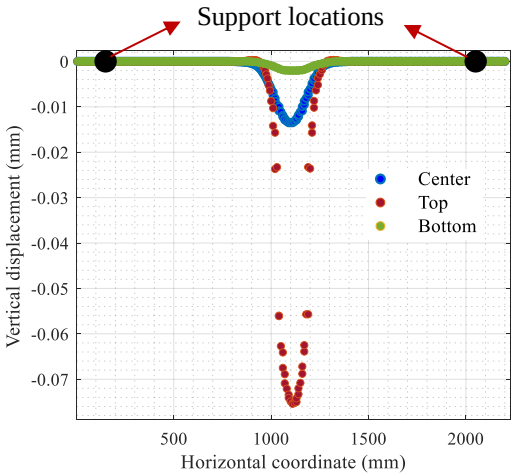

(a) t_1 = 0.75 ms

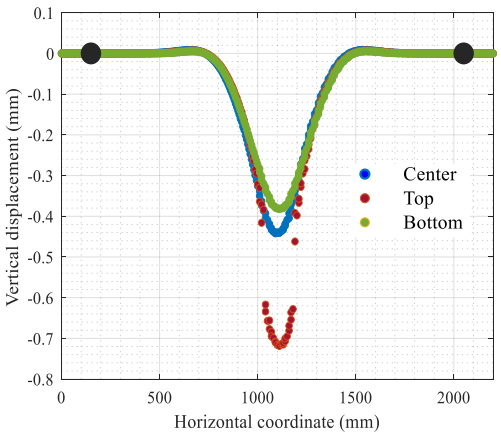

(b) t_2 = 0.9 ms

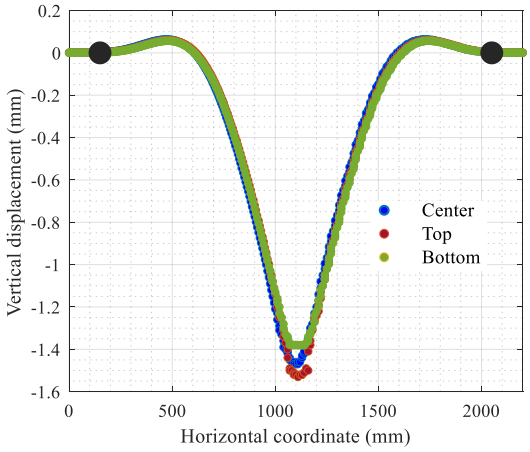

(c) t_3 = 1.05 ms

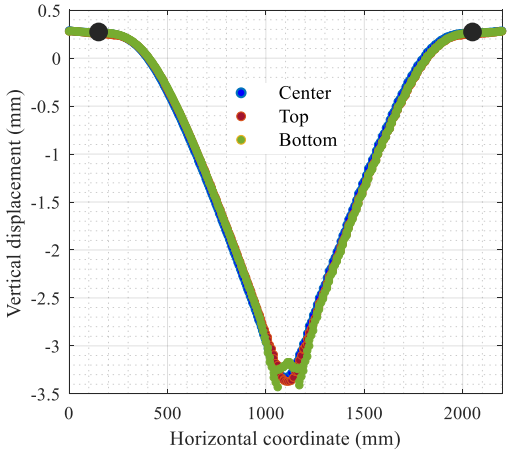

(d) t_4 =1.4 ms

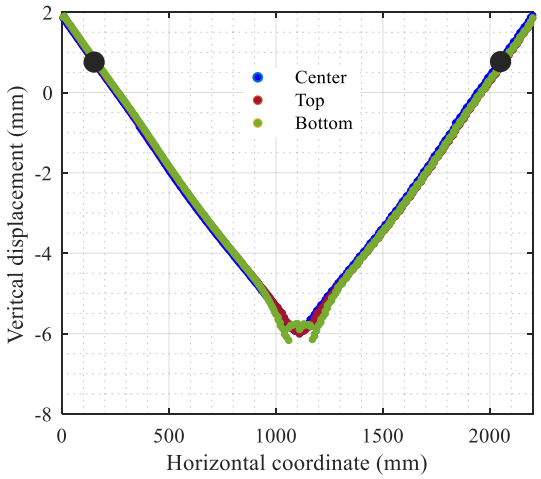

(e) t_5 = 1.8 ms

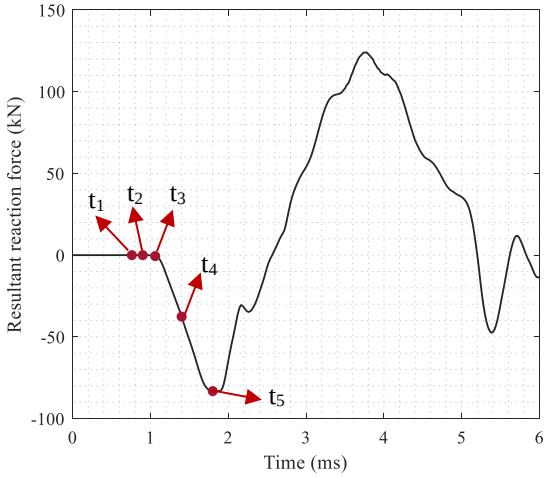

(f) Resultant reaction force

Fig. 21. Analysis of beam deflection at certain instants (span length =1.9 m, drop-weight mass = 200 kg, and impact velocity = 6.26 m/s)

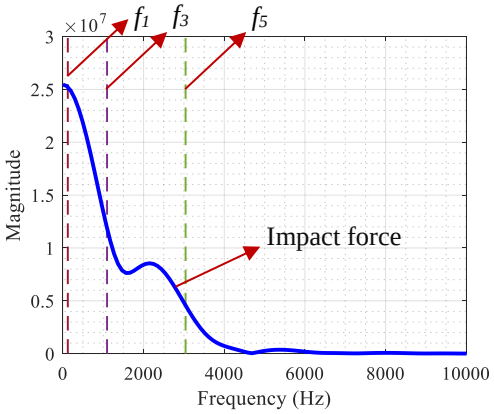

(a) Span length = 1.9 m

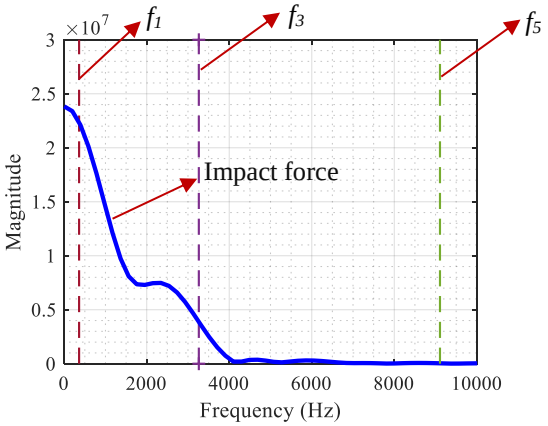

(b) Span length = 1.1 m

Fig. 22. FFT spectrum of impact force

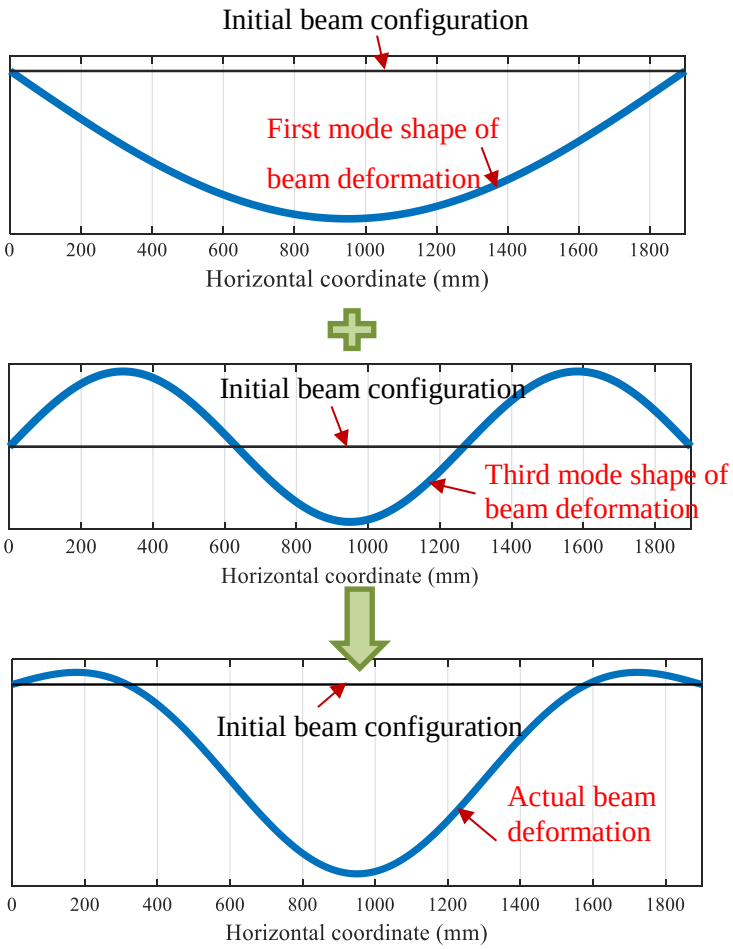

Fig. 23. Mode shapes and resultant deformation shape of the beam at the moment when the negative reaction force activates

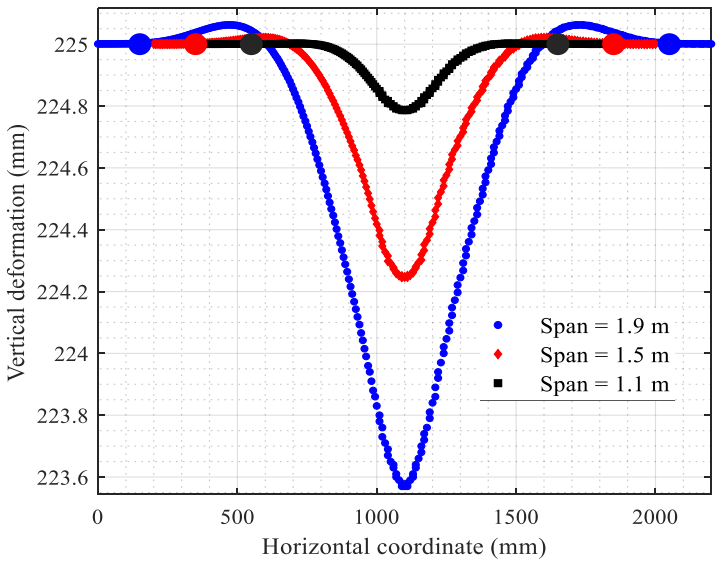

Fig. 24. Comparison of beam deformation at the moment when the negative reaction force activates (drop-weight mass = 200 kg and impact velocity = 6.26 m/s)

3.2. Influence of prestressing at the support

As discussed previously, the negative reaction force of a RC beam subjected to impact loading is caused by the beam deflection but not surface Rayleigh wave. In impact testing, it is not necessary to use the upper load cell to capture the negative reaction force. Using one compression-only load cell placed at the bottom of RC beams together with prestressed bolts is sufficient to capture both the negative and positive reaction forces as used in the previous studies [2, 3]. It is noted that the prestress force in the bolts should be greater than the expected negative reaction force if a compression-only load cell is used to ensure that the load cell is always in compression. However, when prestress force is applied to the bolts at the supports, it generates friction force on the beam and thus more restraint. Accordingly, the additional restraint induced by the prestressed bolts affects the beam response under impact loads, i.e. the vibration and displacement of the beams. It is worth mentioning that the peak impact force is governed by the contact stiffness and the interaction between the beam and the drop-weight [4, 5] while the boundary condition does not affect the peak impact force as confirmed by the previous studies [44, 45]. Therefore, only the beam responses were investigated with respect to the different prestress forces of the bolts. Based on the validated numerical model, the beam design and impact energy remain the same for all cases while the prestress force at each support of four bolts varied from 20 kN to 40 kN.

The numerical model of the beam from the previous study [4] was modified by applying four prestressed bolts at the supports as shown in Fig. 25. The beam had a span of 1.9 m, width of 150 mm, and height of 250 mm. To apply the prestress load on the bolts, the method with the thermal-induced load was adopted by using the keyword *DYNAMIC RELAXATION to generate the prestress force in the bolts. The detailed procedure can be found in the previous study [53]. The numerical results have shown that applying the prestress force (20 kN) could

decrease the maximum displacement by approximately 10% and also reduced the residual displacement by about 11% compared to the case without prestressing force (see Fig. 26). Such a phenomenon occurring in the beam with prestressed bolts at supports can be attributed to the higher friction forces and more restraint. When a larger prestressing force is applied to the bolts, it induces a larger friction force, which might further constrain the beam's rotation. As shown, increasing the prestress force from 20 kN to 40 kN led to a slight decrease in the displacement response (see Fig. 26). This observation suggests that if a prestress force is required to overcome the negative reaction force so that one load cell can measure both negative and positive reaction forces, its effect on the beam deformation and boundary condition is considerable. Therefore, it should be carefully considered and the prestressing force should be reported as a parameter of the boundary condition for detailed analysis of the testing results and verifications of numerical models.

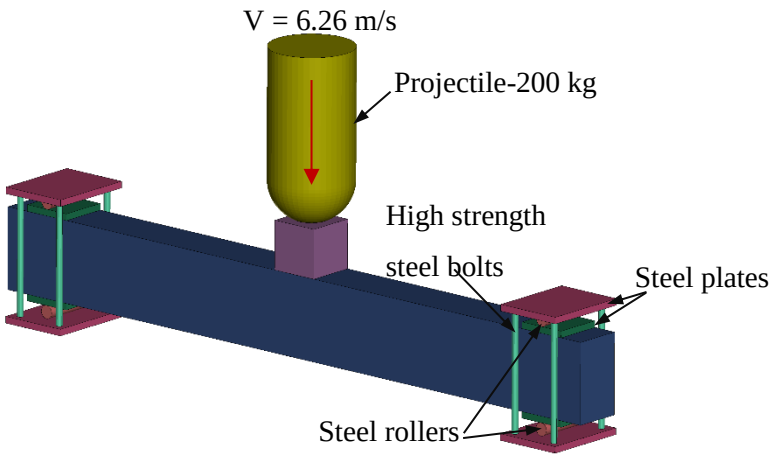

Fig. 25. The model with prestressed bolts at support

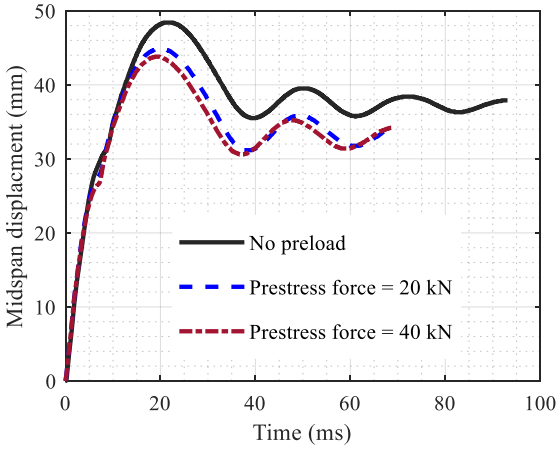

Fig. 26. Effect of prestress force on displacement response (span length =1.9 m, drop-weight mass = 200 kg, and impact velocity = 6.26 m/s)

3.3. Influence of steel plates and friction coefficient

In addition to the prestressed bolts, the setup of a simply-supported beam under impact loads requires rollers [2, 38] and optional steel plates on top of the rollers [1, 6]. This minor variation of the test setup at the support results in different rotating points at the interfaces between the beam and the roller as shown in Fig. 27(a). When only the rollers are used, the rotating causes friction force between concrete and steel while friction between steel and steel happens when rollers are utilized together with steel plates (see Fig. 27(b)). It is noted that the friction coefficient between concrete and steel is different from that between steel and steel. In static tests, there are no prestressed bolts at the support and thus the friction force is small while the prestress force of the bolts may cause a much larger friction force and thus more restraint to the beam. Therefore, the setup of the support does not cause a considerable difference in the beam's response under quasi-static loads but may have a considerable influence on the beam's response under impact loads. To evaluate the effect of using rollers and steel plates on the impact response of RC beams, the 3D FE model as shown in Fig. 27 was modified by removing the steel plates underneath steel rollers and 20 kN prestress force was adopted and referred as Setup 1 (see Fig. 27(a)). The parameters for modelling the contact at the supports are presented in Table 2. Meanwhile the prestressed model as presented in the previous section and Fig. 25

represents the Setup 2 (see Fig. 27(b)) with both rollers and steel plates. The beam had a span of 1.9 m, width of 150 mm, and height of 250 mm. The numerical results have shown that the displacement response of the beam adopting Setup 1 was higher than the counterpart associated with Setup 2, i.e. Setup 2 reduced the maximum displacement by 11% and the residual displacement by 12% as compared with Setup 1. This reduction can be attributed to different friction forces and constraint conditions associated with the two setups. It is noted that with Setup 1 where only rollers were used, the maximum compressive stress of concrete reached 40 MPa. If a higher prestress force is used, local concrete damage may happen at the rollers. Therefore, it is recommended that Setup 2 with the steel plates between the roller and concrete surface should be adopted to distribute the concentrated stress for avoiding concrete damage, but the steel plates impose additional constraint which reduces the beam responses. For accurate assessment and interpretation of testing results, this information should be reported clearly in an experimental study. Accordingly, a similar detailed setup should be modelled in simulation to accurately reflect the actual condition in the experimental tests.

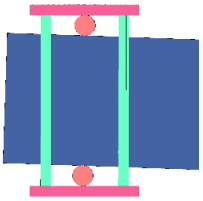

(a) Setup 1

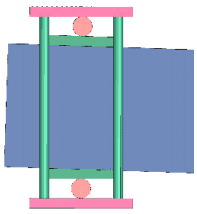

(b) Setup 2

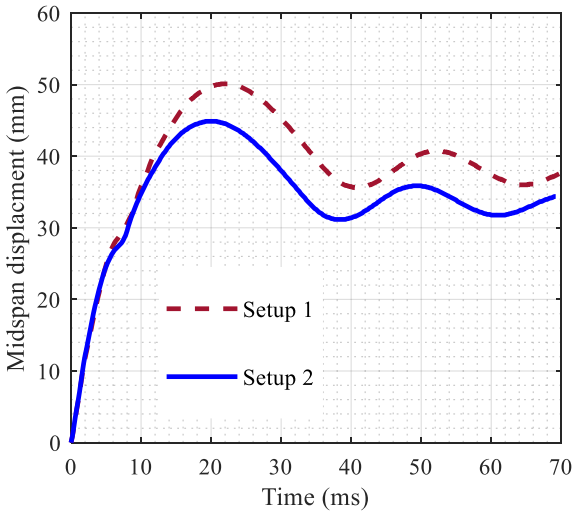

(c) Time histories of displacement

Fig. 27. Effect of different setup conditions on displacement response (span length =1.9 m, drop-weight mass = 200 kg, and impact velocity = 6.26 m/s)

Table 2. Parameters for contact modelling at supports

Contact	SFS/SFM	Static friction coefficient	Dynamic friction coefficient
Steel rollers (SFS)/Steel plates (SFM)	1/1	0.8	0.6
Steel rollers (SFS)/Concrete (SFM)	0.1/0.001	0.6	0.3

*SFS: scale factor of slave elements and *SFM: scale factor of master elements

In addition to the setup of the support, the friction coefficient also affects the beam response and thus the static friction coefficient between steel plates and concrete surface in the second setup was varied from 0.2 to 0.6 to quantify its effect on the impact response of the beams. The static friction coefficient between steel rollers and steel plates was kept at 0.8 for all cases. The friction coefficient was set in keyword *CONTACT_AUTOMATIC_SURFACE_TO_SURFACE. As can be seen in Fig. 28, when increasing the friction coefficient of steel-concrete interface from 0.2 to 0.4, the maximum displacement reduced by 6% and the residual displacement decreased by 8%. Meanwhile, increasing the friction coefficient of steel-concrete interface to 0.6 led to a negligible effect on the displacement of the beams. The numerical results demonstrated that the displacement response of the beams is negligibly affected when the friction coefficient is higher than 0.6. When lubrication is adopted in the interface of steel plates and concrete beams, the static friction coefficient can decrease to 0.2 and therefore, the displacement response of the beams may change slightly. In general, the use of steel plates affects the displacement response but it mitigates stress concentration at the support, and the friction coefficient has a minor influence on the beam displacement. It is suggested that both rollers and steel plates should be used to avoid local damage of concrete.

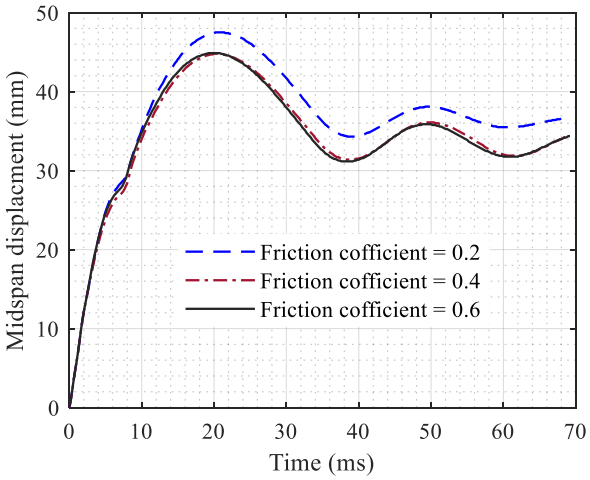

Fig. 28. Effect of friction on the displacement of beams

4. Data processing and energy absorption

4.1 Data filtering

Data acquisition and data processing in impact tests are very important since it may lead to misleading data interpretation or discussions. Very limited studies or discussions about data acquisition are documented in the literature. Many studies just reported the raw data without filtering [1, 3] while some investigations used the average window methods [38], low-pass fourth-order Butterworth filter [54], or cut-off frequency [55-57]. Wang et al. [55] plotted the spectrum of acceleration and found that the frequencies of the governed vibration modes were concentrated in the range of 0-6.2 kHz and 6.2 kHz therefore could be used as a cut-off frequency. Wu et al. [56] also used the frequency-domain analysis for acceleration, velocity, and displacement and suggested the cut-off frequency of 5 kHz. Meanwhile, Remennikov et al. [54] used the Butterworth filter with the cut-off frequency of 1.65 kHz based on ISO 6487:2015 [58]. Pham et al. [51] carried out a spectrum analysis of the impact force and suggested that a cut-off frequency of 5 kHz should be used to avoid filtering out the high impulsive peaks. From these analyses, it can be suggested that a low pass with a cut-off frequency of about 5 kHz should be used for data processing to achieve reasonable outcomes. However, it should be noted

that this suggestion is valid only for low-velocity drop-weight impact tests on RC beams normally conducted in a structural engineering laboratory. For high-velocity impact tests, a higher cut-off frequency should be used.

4.2. Energy absorption

During an impact event, the energy imparted into the beams or so-called imparted energy consists of absorbed energy including deformation and fracture energy and kinetic energy due to beam vibration. When the energy loss is ignored, the external work done by impact force is equal to the variation of the kinetic energy of the drop-weight as shown in Eq. (3).

$$\frac{1}{2}M(V_1^2 - V(t)^2) = W(t) \tag{3}$$

where M is the mass of the projectile, V_1 is the initial impact velocity of the drop-weight , $V(t)$ is the impact velocity of drop hammer at a certain moment t, and $W(t)$ is external work done by impact force. It should be noted that Eq. (3) is valid since the drop-weight is considered as rigid during collision and therefore the internal deformation energy of the drop-weight can be neglected. By using Eq. (3), the imparted energy can be also calculated based on the velocity of the drop-weight which can be recorded by using a high-speed camera. From this point of view, there are two methods to determine the imparted energy: Method 1 integrates the impact force vs displacement curve and Method 2 determines the variation in kinetic energy of the projectile.

Method 1 has been adopted in the previous experimental investigations of reinforced concrete structures subjected to impact loading [1, 2, 28, 38, 59, 60]. In some cases when the beams suffered from severe damage and fragmented into several parts or there was a long separation period of the projectile and the beam, the external work-done by impact force obtained from Method 1 differed significantly from the variation of the kinetic energy of projectile calculated

from Eq. (3) [15, 61]. It can be explained by the fact that after splitting into several parts, the measured mid-span displacement did not represent the actual displacement at the mass center of the entire beam. Furthermore, after suffering from the initial impact, the geometrical configuration of the beam may change significantly due to the severe damage and fragmentation. Therefore, the projectile collided with the beam in an inclination, and thus the impact force was exerted at an angle to the measured vertical displacement. This angle is difficult to be considered in calculation and usually ignored. This can lead to an inaccurate calculation of work done by impact force. To eliminate those errors, Method 2 was adopted and show reasonable results even in the cases of severely splitting and fragmented beams [15]. This is because the calculation of Method 2 is independent of the geometrical configuration of the beams which can be varied during an impact event.

Another critical aspect is to determine the portion of energy absorbed in the forms of deformation and fracture of the beams. Previous studies determined the absorbed energy by integrating the area under the curve of total reaction force (sum of two reaction forces at both supports) and midspan displacement [2, 38, 62] (see Fig. 29), so called Method 3. In that method, the area under the negative phase of the reaction force is excluded in the integration since the negative value of energy cannot exit. Therefore, Method 3 cannot consider the deformation energy absorbed in the beams during the duration of the negative reaction force. To quantify the energy transferred into the beams, the numerical results of the beam adopted from the previous study [4] are presented in Fig. 30. It can be seen from the figure, the energy due to the negative phase of reaction force was approximately 1100 J (33% of the total absorbed energy of the beam). Besides the negative reaction force, there is always a slight delay in activating the reaction force of a beam subjected to impact load. This means while the reaction force is still zero, beam has already started to deform and even suffer certain level of damage. All these would absorb energy but could not be countered by using the method of area enclosed

by the reaction force and midspan displacement. Such a large portion of energy cannot be considered in the calculation indicating Method 3 is questionable. The imparted energy should be estimated by the variation of the kinetic energy (Method 2) rather than integrating the reaction force-displacement curve. To sum up, the conventional Method 1 and Method 3 based on the enclosed area of impact force and reaction force vs displacement curves might be suitable for structures with relatively slow responses and also maintain the initial configuration during the impact.

Fig. 30 shows that 85% of the input kinetic energy was transferred into the absorbed energy of the beams while the remained energy was mainly dissipated by friction and absorbed in the deformation of the adaptor and other setup parts. The evaluation of energy absorbed in different components of the beams, including concrete and steel reinforcements, is presented in Fig. 31. As can be seen from the figure, the energy was mostly absorbed in the deformation of bottom reinforcing bars and followed by the damage of concrete. This can be attributed to the flexural failure mode of the beam where a large portion of the energy was absorbed by tension strain of reinforcing bars and concrete crushing at compression zone. Meanwhile, the contribution to the energy absorption of top reinforcing bars and stirrups in flexural mode was insignificant.

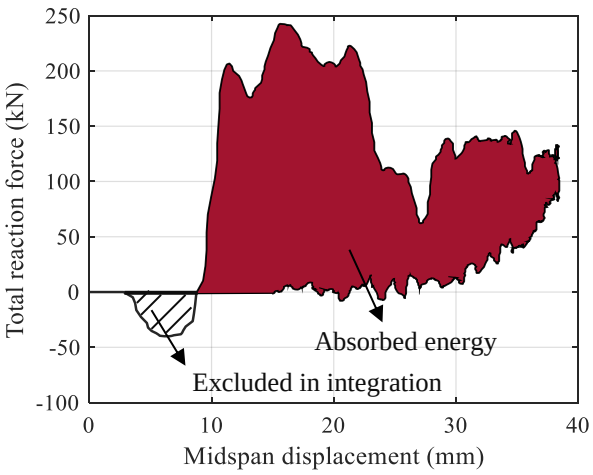

Fig. 29. The method to estimate absorbed energy based on experimental data of reaction force

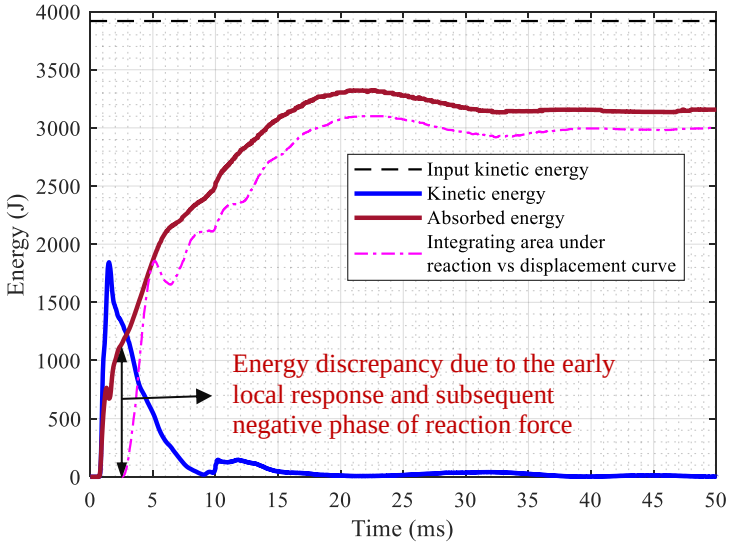

Fig. 30. Evaluation of forms of energy imparted in the beam

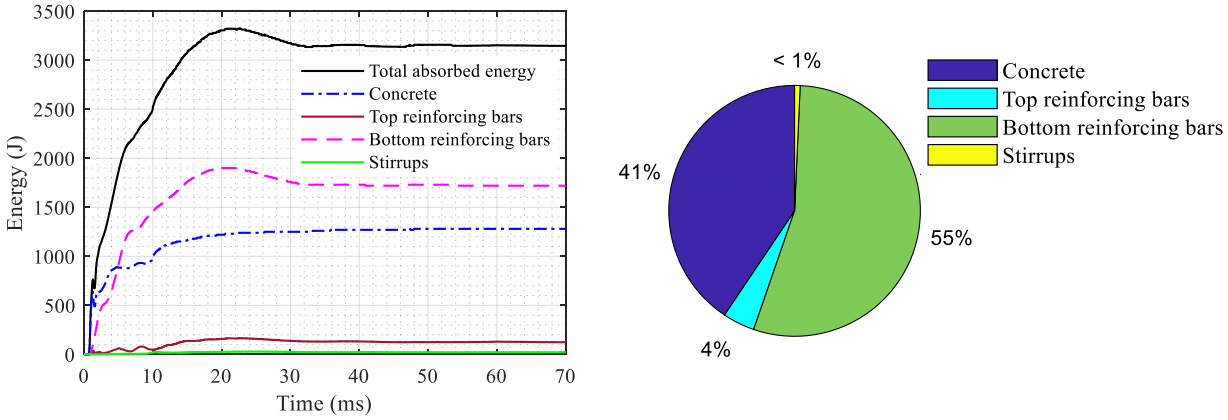

Fig. 31. Evaluation of absorbed energy in different components of the beams

5. Conclusions

This study examines and discusses the effect of various factors and test setup on the impact response of RC beams and the measured data in impact tests. The effects of these factors have not been clarified comprehensively and thus relevant suggestions have not been made yet in the literature. From the above results and analyses, the following conclusions and suggestions can be made:

1. With respect to the load cell embedded in drop-weight, the measured impact force is not accurate if the drop-weight mass ratio (α_d), i.e. the weight above the embedded load cell over the mass of impact head, is lower than 20. Placing the load cell on the beam increases the local contact stiffness and leads to a higher impact force peak and shorter duration than the direct impact.

2. The drop-weight head with a larger contact area causes a higher peak impact force and loading rate. For the drop-weight with a flat head, the initial inclination angle of drop-weight induces a lower peak force due to the decrease of the contact area. In addition, a harder local contact condition by using a steel plate induces an impulse with a higher impact peak and shorter duration and vice versa.

3. The impact force profile can be controlled by adjusting the ratio (α) of the drop-weight mass to the beam mass.

4. The impulse with higher peak force and shorter duration is prone to induce shear-governed failure or punching shear failure and concrete damage at the negative bending moment regions.

5. The negative reaction force is caused by the deformation of RC beams associated with high-order vibration mode.

6. For the setup of the support, one compression-only load cell is sufficient to capture both negative and positive reaction forces by prestressing the load cell. However, prestress force in the bolts affects the beam's response. Using steel plates with rollers at the prestressed support avoids local damage of concrete, but induces a higher level of boundary constraint and reduces the displacement response.

7. A low-pass filter with a frequency of at least 5 kHz should be used for data processing of low-velocity drop-weight tests normally conducted in structural engineering laboratory.

8. When calculating the energy absorption of RC beams under impact loads, using the enclosed area under either the reaction force vs displacement or impact force vs displacement curves may cause a considerable error. The imparted energy, which quantifies the input and output energies, should be used for the energy absorption analysis.

6. Acknowledgement

This study is financially supported by Australian Research Council via Laureate Fellowship Grant No FL180100196.

7. References

[1] Saatci S and Vecchio FJ, Effects of shear mechanisms on impact behavior of reinforced concrete beams, ACI Struct. J. 2009;106 (1):78-86.
[2] Kishi N, Mikami H, Matsuoka K, and Ando T, Impact behavior of shear-failure-type RC beams without shear rebar, Int. J. Impact Eng. 2002;27 (9):955-968.
[3] Fujikake K, Li B, and Soeun S, Impact response of reinforced concrete beam and its analytical evaluation, J. Struct. Eng. 2009;135 (8):938-950.
[4] Pham TM, Hao Y, and Hao H, Sensitivity of impact behaviour of RC beams to contact stiffness, Int. J. Impact Eng. 2018;112:155-164.
[5] Pham TM and Hao H, Influence of global stiffness and equivalent model on prediction of impact response of RC beams, Int. J. Impact Eng. 2018;113:88-97.
[6] Cotsovos DM, A simplified approach for assessing the load-carrying capacity of reinforced concrete beams under concentrated load applied at high rates, Int. J. Impact Eng. 2010;37 (8):907-917.
[7] Erki M and Meier U, Impact loading of concrete beams externally strengthened with CFRP laminates, J. Compos. Constr. 1999;3 (3):117-124.
[8] Yu R, van Beers L, Spiesz P, and Brouwers HJH, Impact resistance of a sustainable Ultra-High Performance Fibre Reinforced Concrete (UHPFRC) under pendulum impact loadings, Constr. Build. Mater. 2016;107:203-215.
[9] Pham TM and Hao H, Behavior of fiber reinforced polymer strengthened reinforced concrete beams under static and impact loads, Int. J. Protect. Struct. 2017;8 (1):1-22.
[10] Pham TM and Hao H, Impact behavior of FRP-strengthened RC beams without stirrups, J. Compos. Constr. 2016;20 (4):04016011.
[11] Anil Ö, Durucan C, Erdem RT, and Yorgancilar MA, Experimental and numerical investigation of reinforced concrete beams with variable material properties under impact loading, Constr. Build. Mater. 2016;125:94-104.

[12] Li H, Chen W, and Hao H, Influence of drop weight geometry and interlayer on impact behavior of RC beams, Int. J. Impact Eng. 2019;131:222-237.
[13] Li H, Chen W, and Hao H, Factors influencing impact force profile and measurement accuracy in drop weight impact tests, Int. J. Impact Eng. 2020:103688.
[14] Kishi N and Bhatti AQ, An equivalent fracture energy concept for nonlinear dynamic response analysis of prototype RC girders subjected to falling-weight impact loading, Int. J. Impact Eng. 2010;37 (1):103-113.
[15] Pham TM, Chen W, Elchalakani M, Karrech A, and Hao H, Experimental investigation on lightweight rubberized concrete beams strengthened with BFRP sheets subjected to impact loads, Eng. Struct. 2020;205:110095.
[16] Li H, Chen W, Pham TM, and Hao H, Analytical and numerical studies on impact force profile of RC beam under drop weight impact, Int. J. Impact Eng. 2021;147:103743.
[17] Zhao D, Yi W, and Kunnath SK, Shear mechanisms in reinforced concrete beams under impact loading, J. Struct. Eng. 2017;143 (9):04017089.
[18] Li H, Chen W, and Hao H, Dynamic response of precast concrete beam with wet connection subjected to impact loads, Eng. Struct. 2019;191:247-263.
[19] Do TV, Pham TM, and Hao H, Impact force profile and failure classification of reinforced concrete bridge columns against vehicle impact, Eng. Struct. 2019;183:443-458.
[20] Yoo D-Y, Banthia N, Kim S-W, and Yoon Y-S, Response of ultra-high-performance fiber-reinforced concrete beams with continuous steel reinforcement subjected to low-velocity impact loading, Compos. Struct. 2015;126:233-245.
[21] Huynh L, Foster S, Valipour H, and Randall R, High strength and reactive powder concrete columns subjected to impact: Experimental investigation, Constr. Build. Mater. 2015;78:153-171.
[22] Isaac P, Darby A, Ibell T, and Evernden M, Experimental investigation into the force propagation velocity due to hard impacts on reinforced concrete members, Int. J. Impact Eng. 2017;100:131-138.
[23] Yoo D-Y and Banthia N, Size-dependent impact resistance of ultra-high-performance fiber-reinforced concrete beams, Constr. Build. Mater. 2017;142:363-375.
[24] Huh H, Lim JH, and Park SH, High speed tensile test of steel sheets for the stress-strain curve at the intermediate strain rate, International Journal of Automotive Technology 2009;10 (2):195-204.
[25] Dey V, Bonakdar A, and Mobasher B, Low-velocity flexural impact response of fiber-reinforced aerated concrete, Cem. Concr. Compos. 2014;49:100-110.
[26] Ulzurrun GSD and Zanuy C, Enhancement of impact performance of reinforced concrete beams without stirrups by adding steel fibers, Constr. Build. Mater. 2017;145:166-182.
[27] Wang W, Wu C, Li J, Liu Z, and Lv Y, Behavior of ultra-high performance fiber-reinforced concrete (UHPFRC) filled steel tubular members under lateral impact loading, Int. J. Impact Eng. 2019;132:103314.
[28] Kishi N, Komuro M, Kawarai T, and Mikami H, Low-velocity impact load testing of RC beams strengthened in flexure with bonded FRP sheets, J. Compos. Constr. 2020;24 (5):04020036.
[29] Nghiem A and Kang TH-K, Drop-weight testing on concrete beams and aci design equations for maximum and residual deflections under low-velocity impact, ACI Struct. J. 2020;117 (2).
[30] Adhikary SD, Li B, and Fujikake K, Low velocity impact response of reinforced concrete beams: Experimental and numerical investigation, Int. J. Protect. Struct. 2015;6 (1):81-111.
[31] Yilmaz M, Anil Ö, Alyavuz B, and Kantar E, Load displacement behavior of concrete beam under monotonic static and low velocity impact load, International Journal of Civil Engineering 2014;12 (4):488-503.

[32] Guo J, Cai J, Chen Q, Liu X, Wang Y, and Zuo Z, Dynamic behaviour and energy dissipation of reinforced recycled aggregate concrete beams under impact, Constr. Build. Mater. 2019;214:143-157.
[33] Saleh Z, Sheikh MN, Remennikov A, and Basu A, Damage assessment of GFRP bar reinforced ultra-high-strength concrete beams under overloading impact conditions, Eng. Struct. 2020;213:110581.
[34] Jin L, Zhang R, Dou G, Xu J, and Du X, Experimental and numerical study of reinforced concrete beams with steel fibers subjected to impact loading, International Journal of Damage Mechanics 2018;27 (7):1058-1083.
[35] Yan Q, Sun B, Liu X, and Wu J, The effect of assembling location on the performance of precast concrete beam under impact load, Adv. Struct. Eng. 2018;21 (8):1211-1222.
[36] Tachibana S, Masuya H, and Nakamura S, Performance based design of reinforced concrete beams under impact, Natural Hazards and Earth System Science 2010;10 (6):1069-1078.
[37] Wang H, Yang B, Zhou X, and Kang S, Numerical analyses on steel beams with fin-plate connections subjected to impact loads, Journal of Constructional Steel Research 2016;124:101-112.
[38] Kishi N and Mikami H, Empirical formulas for designing reinforced concrete beams under impact loading, ACI Struct. J. 2012;109 (4):509-519.
[39] Zhan T, Wang Z, and Ning J, Failure behaviors of reinforced concrete beams subjected to high impact loading, Eng. Fail. Anal. 2015;56:233-243.
[40] Chen Y and May IM, Reinforced concrete members under drop-weight impacts, Proceedings of the ICE-Structures and Buildings 2009;162 (1):45-56.
[41] Zhao D, Yi W, and Kunnath SK, Numerical simulation and shear resistance of reinforced concrete beams under impact, Eng. Struct. 2018;166:387-401.
[42] Bhatti AQ, Kishi N, Konno H, and Mikami H, Elasto-plastic dynamic response analysis of prototype RC girder under falling-weight impact loading considering mesh size effect, Structure and Infrastructure Engineering 2012;8 (9):817-827.
[43] Huang Z, Chen W, Hao H, Chen Z, Pham TM, Tran TT, and Elchalakani M, Flexural Behaviour of Ambient Cured Geopolymer Concrete Beams Reinforced with BFRP Bars under Static and Impact Loads, Composite structures 2021;Accepted.
[44] Pham TM and Hao H, Effect of the plastic hinge and boundary condition on the impact behaviour of RC beams, Int. J. Impact Eng. 2017;102:74-85.
[45] Pham TM and Hao H, Plastic hinges and inertia forces in RC beams under impact loads, Int. J. Impact Eng. 2017;103:1-11.
[46] Yang Y, Lam N, and Zhang L, Estimation of response of plate structure subject to low velocity impact by a solid object, International Journal of Structural Stability Dynamics 2012;12 (06):1250053.
[47] Zhao W and Qian J, Resistance mechanism and reliability analysis of reinforced concrete columns subjected to lateral impact, Int. J. Impact Eng. 2020;136:103413.
[48] Hao H, Predictions of structural response to dynamic loads of different loading rates, Int. J. Protect. Struct. 2015;6 (4):585-606.
[49] Fu Y, Yu X, Dong X, Zhou F, Ning J, Li P, and Zheng Y, Investigating the failure behaviors of RC beams without stirrups under impact loading, Int. J. Impact Eng. 2020;137:103432.
[50] Hallquist JO, LS-DYNA theory manual, Livermore software Technology corporation 2006;3:25-31.
[51] Pham TM, Chen W, and Hao H, Review on Impact Response of Reinforced Concrete Beams: Contemporary Understanding and Unsolved Problems, Advances in Structural Engineering 2020;Revision submitted.

[52] Roark RJ, Young WC, Budynas RG, and Sadegh AM, Roark's formulas for stress and strain, 8th ed. ed., New York: McGraw-Hill, New York, 2012.
[53] Do TV, Pham TM, and Hao H, Numerical investigation of the behaviour of precast segmental concrete columns subjected to vehicle collision, Eng. Struct. 2018;156:375-393.
[54] Remennikov AM, Kong SY, and Uy B, The response of axially restrained non-composite steel–concrete–steel sandwich panels due to large impact loading, Eng. Struct. 2013;49:806-818.
[55] Wang N, Mindess S, and Ko K, Fibre reinforced concrete beams under impact loading, Cem. Concr. Res. 1996;26 (3):363-376.
[56] Wu M, Chen Z, and Zhang C, Determining the impact behavior of concrete beams through experimental testing and meso-scale simulation: I. Drop-weight tests, Engineering Fracture Mechanics 2015;135:94-112.
[57] Liu T and Xiao Y, Impact behavior of CFRP-strip–wrapped RCbeams without stirrups, J. Compos. Constr. 2017;21 (5):04017035.
[58] ISO 6487:2015, Road vehicles: measurement techniques in impact tests: Instrumentation, in, International Organization for Standardization, 1987.
[59] Zhang X, Hao H, and Li C, Experimental investigation of the response of precast segmental columns subjected to impact loading, Int. J. Impact Eng. 2016;95:105-124.
[60] Pham TM, Zhang X, Elchalakani M, Karrech A, Hao H, and Ryan A, Dynamic response of rubberized concrete columns with and without FRP confinement subjected to lateral impact, Constr. Build. Mater. 2018;186:207-218.
[61] Tran TT, Pham TM, Huang Z, Chen W, Hao H, and Elchalakani M, Effect of fibre reinforcements on shear capacity of geopolymer concrete beams subjected to impact loads, Int. J. Impact Eng. 2020;Under review.
[62] Tran TT, Pham TM, Huang Z, Chen W, Hao H, and Elchalakani M, Impact response of fibre reinforced geopolymer concrete beams with BFRP bars and stirrups, Eng. Struct. 2021;231:111785.